

DOKUZ EYLÜL UNIVERSITY
GRADUATE SCHOOL OF NATURAL AND APPLIED SCIENCES

**ANALYSIS OF RESONANCE OVERVOLTAGES
IN MEDIUM VOLTAGE LEVEL WITH SIX-STEP
INDUCTION MOTOR DRIVE**

by
Sema Nur İPEK

October, 2019
İZMİR

ANALYSIS OF RESONANCE OVERVOLTAGES IN MEDIUM VOLTAGE LEVEL WITH SIX-STEP INDUCTION MOTOR DRIVE

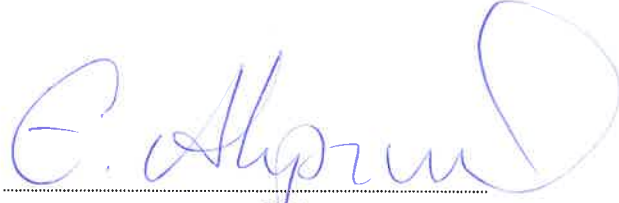
**A Thesis Submitted to the
Graduate School of Natural And Applied Sciences of Dokuz Eylül University
In Partial Fulfillment of the Requirements for the Degree of Master of Science
in Electrical and Electronics Engineering Program**

**by
Sema Nur İPEK**

**October, 2019
İZMİR**


M.Sc THESIS EXAMINATION RESULT FORM

We have read the thesis entitled “ANALYSIS OF RESONANCE OVERVOLTAGES IN MEDIUM VOLTAGE LEVEL WITH SIX-STEP INDUCTION MOTOR DRIVE” completed by SEMA NUR İPEK under supervision of PROF.DR. EYÜP AKPINAR and we certify that in our opinion it is fully adequate, in scope and in quality, as a thesis for the degree of Master of Science.



Prof.Dr. Eyüp AKPINAR

Supervisor




Prof.Dr. Levent Eren

(Jury Member)



Doç.Dr. Engin Karatepe

(Jury Member)



Prof.Dr. Kadriye ERTEKİN

Director
Graduate School of Natural and Applied Sciences

ACKNOWLEDGMENTS

I would like to thank my Supervisor Prof. Dr. Eyup Akpınar for his patience, support and guidance. I will benefit from the perspective that he has given me, and the scientific thinking he has helped me to develop, throughout my life. I'm very happy to have the opportunity to work with him.

Sema Nur İPEK



ANALYSIS OF RESONANCE OVERVOLTAGES IN MEDIUM VOLTAGE LEVEL WITH SIX-STEP INDUCTION MOTOR DRIVE

ABSTRACT

In this thesis, it has been focused on power systems with a six-step 120-degree induction motor drive in medium voltage level. These systems may be preferred instead of PWM based systems in facilities such as geothermal power plants and submarine oil wells where all operations must be maintained with high safety standards, since dead-time control of them is easier. However, due to the harmonics generated by the switching elements they contain and the resonance and overvoltage problems they bring, they can cause hazards that may result in the burnout of the elements. The magnitude of this hazard can further enhance with the effects of the element such as long cables and motors. In these fields, it is important to determine the resonance frequency and prevent it to coincide with any harmonic frequency before the destructive effects are seen, since the maintenance of the elements may be difficult due to the depth or distance at which the element is located. In this thesis, analytical methods and computer simulations are used to determine the resonance frequency. Also, factors that may affect resonance conditions were examined and recommendations were made to reduce the effects of resonance.

Keywords: Six-step drive, 120-degree conduction, induction motor drive, variable frequency drive, resonance overvoltages, LCL filter, C-type filter

ALTI-ADIMLI ASENKRON MOTOR SÜRÜCÜSÜ İLE ORTA GERİLİM SEVİYESİNDE REZONANS AŞIRI GERİLİMLERİNİN ANALİZİ

ÖZ

Bu tezde, orta gerilim seviyesinde, 6-kademeli 120-derece asenkron motor sürücü içeren güç sistemlerine odaklanılmıştır. Bu sistemler, ölü zaman denetimleri daha kolay sağlanabildiği için, bütün işlemlerin yüksek güvenlik standartları ile sürdürülmesini gerektiren jeotermal enerji santralleri ve denizaltı petrol kuyuları gibi tesislerdeki, PWM tabanlı sistemler yerine tercih edilebilmektedir. Bununla birlikte, içerdikleri anahtarlama elemanlarının ürettiği harmonikler ve bunların beraberinde getirdiği rezonans ve aşırı gerilim sorunları nedeniyle, elemanların yanması ile sonuçlanabilecek tehlikelere neden olabilirler. Bu tehlikenin büyüklüğü, kablo ve motor gibi elemanların etkileriyle daha da artabilir. Bu alanlarda, elemanların bakımı bulundukları derinlik veya mesafe nedeniyle zor olabileceğinden, rezonans frekansını belirlenmesi ve tahrip edici etkileri görülmeden önce herhangi bir harmonik frekansla çakışmasının önlenmesi önemlidir. Bu tezde rezonans frekansını belirlemek için analitik yöntemler ve bilgisayar simülasyonları kullanılmıştır. Ayrıca, rezonans koşullarını etkileyebilecek faktörler incelenmiş ve rezonansın etkilerini azaltmak için önerilerde bulunulmuştur.

Anahtar kelimeler: Altı-kademeli sürücü, 120-derece iletim modu, asenkron motor sürücü, değişken frekanslı sürücü, rezonans aşırı gerilimleri, LCL filtre, C-tip filtre

CONTENTS

	Page
M.Sc THESIS EXAMINATION RESULT FORM.....	ii
ACKNOWLEDGEMENTS.....	iii
ABSTRACT.....	iv
ÖZ.....	v
LIST OF FIGURES.....	viii
LIST OF TABLES.....	x
CHAPTER ONE – INTRODUCTION.....	1
CHAPTER TWO – STRUCTURE OF THE SYSTEM.....	5
2.1 Components of the System.....	7
2.1.1 Driver Group.....	7
2.1.1.1 12-Pulse Rectifier.....	7
2.1.1.2 DC Link.....	11
2.1.1.3 Six-Step (Square-wave) Inverter.....	12
2.1.2 Load Group.....	17
2.1.2.1 Step-up Transformer.....	17
2.1.2.2 The Power Cables.....	18
2.1.2.3 The Induction Motor.....	21
2.2 Per-unit Conversion for the System Parameters.....	23
2.3 Simulation of the System.....	36
CHAPTER THREE – RESONANCE ANALYSIS.....	42
3.1 Determination of Resonance Frequency.....	43
3.1.1 Solution Method with the Reactive Component of the Impedance.....	43
3.1.2 Bode Diagram.....	47
3.1.3 General Resonance Frequency Formula.....	48

	Page
3.1.4 FFT Analysis.....	49
3.2 Factors Affecting Resonance Conditions.....	52
3.2.1 Effects of Cable Length on Resonance.....	52
3.2.2 Effects of Motor Slip on Resonance.....	55
3.3 Resonance Conditions during Acceleration of the Motor.....	57
 CHAPTER FOUR – SYSTEM PROTECTION AGAINST RESONANCE.....	 66
4.1 LCL Filter.....	66
4.2 C-Type Filter.....	74
 CHAPTER FIVE – CONCLUSIONS.....	 78
 REFERENCES.....	 79
 APPENDICES.....	 84
Appendix 1: MATLAB Script for Per-unit Data.....	84
Appendix 2: MATLAB Script for Calculation of the Resonance Frequency.....	87
Appendix 3: MATLAB Script for Calculation of Total Parameters.....	88
Appendix 4: MATLAB Script for Determination of Resonance Statuses.....	89

LIST OF FIGURES

	Page
Figure 2.1 Single line diagram of the power system.....	6
Figure 2.2 Structure of the 12-pulse rectifier.....	8
Figure 2.3 Output voltage waveforms of the rectifier.....	9
Figure 2.4 Input current of the first rectifier group.....	10
Figure 2.5 Input current of the second rectifier group.....	10
Figure 2.6 Input current of the 12-pulse rectifier group.....	11
Figure 2.7 The waveform of the rectifier output voltage after using the capacitor...12	12
Figure 2.8 The structure of 6-step inverter.....	12
Figure 2.9 Logical transition circuit between 120-degree and 180-degree conduction modes.....	13
Figure 2.10 Gate signals in 120-degree conduction.....	14
Figure 2.11 Phase-neutral in 120-degree conduction.....	14
Figure 2.12 Phase-phase in 120-degree conduction.....	14
Figure 2.13 Gate signals in 180-degree conduction.....	15
Figure 2.14 Phase-neutral in 180-degree conduction.....	15
Figure 2.15 Phase-phase in 180-degree conduction.....	15
Figure 2.16 Scalar control.....	16
Figure 2.17 The equivalent circuit of the transformer referred to primary side.....	17
Figure 2.18 Simplified equivalent circuit of the transformer.....	18
Figure 2.19 Structure of the power cable.....	19
Figure 2.20 Simplified power cable equivalent circuit.....	19
Figure 2.21 Simplified equivalent circuit of the induction motor.....	22
Figure 2.22 Zones of the system.....	24
Figure 2.23 The analyzed 3-phase medium voltage power system.....	36
Figure 2.24 Output current and voltage waveforms of the 12-pulse rectifier.....	38
Figure 2.25 Output line-to-line voltage waveforms of the inverter.....	38
Figure 2.26 Output current waveforms of the inverter.....	39
Figure 2.27 Voltage waveforms of the motor terminals.....	39
Figure 2.28 Stator current waveforms of the motor (with no load).....	40

	Page
Figure 2.29 Stator current waveforms of the motor (with load).....	40
Figure 2.30 Torque and speed graphs of the motor.....	41
Figure 2.31 The relationship between torque and speed at different frequencies.....	41
Figure 3.1 Load model of the system.....	44
Figure 3.2 The simplified load model.....	44
Figure 3.3 Norton equivalent circuit of the load model.....	44
Figure 3.4 The analyzed load model.....	45
Figure 3.5 Bode diagram.....	47
Figure 3.6 FFT analysis of motor terminal voltage.....	51
Figure 3.7 FFT analysis of inverter output current.....	51
Figure 3.8 Bode diagram results according to various cable lengths.....	52
Figure 3.9 FFT results according to various cable lengths.....	53
Figure 3.10 Change of resonance frequency according to cable length.....	54
Figure 3.11 Bode diagram results at different slip values.....	55
Figure 3.12 Slip and resonance frequency change.....	57
Figure 3.13 Torque and speed graphs at various frequencies a) 3 Hz b) 7 Hz c) 13 Hz d) 16 Hz e) 22 Hz.....	58
Figure 3.14 Torque and speed graphs at various frequencies a) 25 Hz b) 30 Hz c) 34 Hz d) 41 Hz e) 48 Hz.....	59
Figure 3.15 Motor terminal voltage and FFT analysis at 16 Hz.....	61
Figure 3.16 Motor terminal voltage and FFT analysis at 25 Hz.....	61
Figure 3.17 Motor terminal voltage and FFT analysis at 34 Hz.....	62
Figure 3.18 Motor terminal voltage and FFT analysis at 41 Hz.....	62
Figure 3.19 Resonance status during start operation of the system.....	65
Figure 4.1 The structure of LCL filter.....	67
Figure 4.2 The filter position.....	67
Figure 4.3 Motor terminal voltage and FFT analysis.....	73
Figure 4.4 Motor terminal voltage and FFT analysis in last state.....	73
Figure 4.5 C-Type filter structure.....	74
Figure 4.6 Motor terminal voltage and FFT analysis.....	77

LIST OF TABLES

	Page
Table 2.1 Electrical parameters of cables (per kilometer).....	25
Table 2.2 Electrical parameters of three-winding step-down transformer.....	25
Table 2.3 Electrical parameters of step-up transformer.....	25
Table 2.4 Electrical parameters of induction motor.....	25
Table 2.5 Value of DC link capacitance.....	25
Table 2.6 Electrical parameter of three-phase voltage source.....	25
Table 2.7 Per-unit electrical parameters of cables (per kilometer).....	35
Table 2.8 Per-unit electrical parameters of three-winding step-down transformer....	35
Table 2.9 Per-unit electrical parameters of step-up transformer.....	35
Table 2.10 Per-unit electrical parameters of induction motor.....	35
Table 2.11 Per-unit electrical parameter of smoothing capacitance.....	35
Table 2.12 Per-unit electrical parameter of three-phase voltage source.....	35
Table 3.1 Slip and root values.....	56
Table 4.1 Parameters of the LCL filter.....	71
Table 4.2 Parameters of the C-type filter.....	77

CHAPTER ONE

INTRODUCTION

In submarine oil wells, geothermal power plants and petrochemical plants, many processes related to the extraction of raw materials from the source are carried out underground or underwater. These processes require the use of high-power electric motors. Because, even if the pressure of the materials is sufficient to initially flush to the surface, it is necessary to use artificial elevation methods as they will decrease over time (Hussain, Anvari & Toliyat, 2017). Electric submersible pumping systems (ESP), containing electric motors, are widely used for this purpose since they are suitable for large-scale processes and have a good cost-efficiency relationship (Liang & Fleming, 2013; Qian et al., 2018). In these systems, brushless DC motors (BLDC/ECM) (Sundaram, Anand, Vinod & Mounya, 2016), permanent magnet synchronous motors (PMSM) (Zheng & Wang, 2013), or induction motors (IM) (Thorsen & Dalya, 2001) can be used. The motors have advantages over each other in terms of efficiency, cost, structure simplicity, and durability. However, in Europe, systems containing induction motors are commonly used, produced by manufacturers such as Baker Hughes (Spijker & Ungemach, 2016).

In these industrial plants, the speed and torque control of the motors is usually provided by variable frequency drives(VFD/VSD) (Takacs, 2009). Due to the control methods, there are different types of variable frequency drives. In particular, modulation and commutation techniques are decisive in classification. In the ESP field, PWM or six-step output waveforms may be useful. However, the iron losses that can be observed in the motor, containing magnetic material, are higher in the PWM driven system due to the pieced output waveform and eddy currents rising (Boglietti, Ferraris, Lazzari & Profumo, 1993). In addition, in PWM, unwanted "shoot through" may occur in the inverter legs and cause unsteadiness in this system. This reveals the necessity of deadtime (Kerkman, Rowan, Leggate & Seibel, 1995) and makes the six-step technique with lower switching frequency more secure for high power levels and large capacity switches (Xu & Ye, 1995). Therefore, it may be preferable to use six-step outputs in these fields that have power systems at MVA levels. This output can also be achieved using different PWM strategies such as

overmodulation (Holtz, Lotzkat & Khambadkone, 1993; Hussen, 2009; Narayanan & Ranganathan, 1998, 2002).

Two commutation techniques, 120-degree conduction and 180-degree conduction, are commonly used in variable frequency drives. However, torque fluctuations in the motor may occur due to inappropriate selection of the current commutation method. Because of the inductance of the motor windings and the effect of reactive power feedback diodes connected in parallel to the inverter switches, current conduction cannot change momentarily, depending on these variables, it requires a certain rise and fall time (Baby & George, 2012). For large, bulky motors in this field, 120-degree conduction with wide time tolerance may be preferred to ensure these times and to operate the engine safely (Sudhoff & Krause, 1990).

In these systems, VFD panels, and transformers that used to shape voltage waveform or adjust voltage magnitude are usually in an above ground control center or substation. The motors located in the wells are supplied with long cables from these centers (Takacs, 2009). In general, these facilities can be classified as an extra hazardous area due to the properties and temperature levels of the extracted materials. All operations at these sites should be carried out with high safety standards. However, the drive systems used contain semiconductor switching elements, which cause them to produce current and voltage harmonics. Because of the capacitive effects of the long cables that increases with their length and the inductive properties of large elements such as motor and transformer, the resonance problems of harmonics come into prominence. The formation of resonance leads to overvoltages and overcurrents. These may cause insulation damage to the motor and cables. Furthermore, this case can result in burnout of the motor or cables. Therefore, it is important to determine the resonance state and to take precautions based on this determination.

Underground mining, submarine oil wells and geothermal power plants create similar industrial environments with long cable and motor drive usage characteristics. The motors are used in mines for grinding, preparation, transportation (Morley, 1990). In addition, they can be used as fans for the ventilation of mines (Rodriguez et al., 2006). Therefore, similar resonance problems and hazards may

also be encountered in these areas. Several studies have previously been made concerning this issue.

Rogriguez et al. (2004) suggested that the causes of overvoltages in the terminals of an asynchronous machine driven by PWM inverter used for ventilation in mines are theoretically oscillation and resonance. They concluded that resonance is the main cause by field measurements. In order to reduce overvoltages, they proposed a second-order low-pass filter design for this system.

Endrejat & Pillay (2009) have studied a system used in large chemical process plants that includes a synchronous motor and a multilevel H-bridge (VSI) inverter drive, by focusing on oscillations and resonance induced overvoltages between the drive and motor. They have created different application scenarios according to the use of synchronization reactor at the inverter output and have made field measurements and simulations. As a result, it is stated that the effects of resonance can be minimized by selecting the appropriate carrier signal frequency for the inverter in a system using this type of drive.

In another study, Endrejat, Burmeister et al. (2009) examined systems containing VSI and LCI synchronous motor drives, taking into account the long cables required by the system and their effects, and concluded that resonance conditions occurred at these cable lengths. They also have made an assessment of when additional electrical filter and rotor position detection equipment may be required and they have proposed an RC filter for the safe operation of the system.

Liang, Kar & Liu (2014) designed a load filter for a submersible pump system with NPC drives by based on the characteristic harmonics of the system. They have confirmed by field measurements that the increased distortion in the event of a resonance that can be caused by the drive-induced harmonics can be reduced by an LC type load filter.

Bertoldi, Pathmanathan, Kanchan, Spiliotis & Driesen (2018) have proposed a 2-level inverter (Q2L) that requires lower capacitor and filter component values to

reduce overvoltages in their work aimed at applications of motor and drive systems connected with long cables.

In this thesis, it has been focused on a power system including a 6-step 120-degree induction motor drive in medium voltage level. The resonance that may occur in this system and the overvoltages caused by the resonance have been analyzed. Analytical methods and computer simulations were used to investigate when resonance conditions would occur. Suggestions were made on how resonance can be prevented.

In the second chapter, the components of the system analyzed are discussed. It has been shown how to convert the system to per-unit as it provides a more comprehensive interpretation. In chapter three, resonance analysis is performed with analytical methods and simulations and the results are examined. In chapter four, filtering methods are proposed to reduce resonance and its effects. Finally, in the conclusion part, general evaluations about resonance and how to prevent resonance have been made.

CHAPTER TWO

STRUCTURE OF THE SYSTEM

Power systems with different characteristics according to their needs can be grouped according to voltage levels. Industrial plants such as mining and petrochemical plants are generally in the group that classified as "AC three-phase systems having a rated voltage above 1 kV and not exceeding 35 kV and related equipment" according to IEC 60038 Standards. It can be said that this group corresponds to the medium voltage level.

In concerned industrial plants, it is not desirable to interrupt production, except for some planned situations called "Downtime". Downtime is performed only in a certain part of the plant to carry out maintenance and renovation work. Raw materials extracted, processed or used in these facilities are generally flammable and explosive. Except in certain cases, such as the burning of materials in the piping in order to clean the pipelines, it is undesirable that even an uncontrolled spark will be generated in the plant. Therefore, it is so important to ensure the continuity and reliability of the processes in these facilities. The power systems of the facilities are also customized accordingly.

Modern power systems consist of four main parts: production, transmission lines, distribution and loads (Saadat, 2010). It is not always appropriate to include these industrial facilities in a classification of individual, commercial and industrial loads. Because, a connection to the interconnected network can be made to meet the power requirements of the system, but plants usually have their own power supplies and even backups (Takacs, 2009). So they can be considered as a separate power system.

The facilities can include main station, substations or control (operator) centers. Transformers and power electronics components are usually found in these centers. The location of generators used as a source is usually close to these centers. Other than this, these facilities can include high pipe racks, chimneys, and vertical pumps. Therefore, transmission lines are generally not used to prevent any danger even in sections above the ground. In these plants, there are underground channels, covered

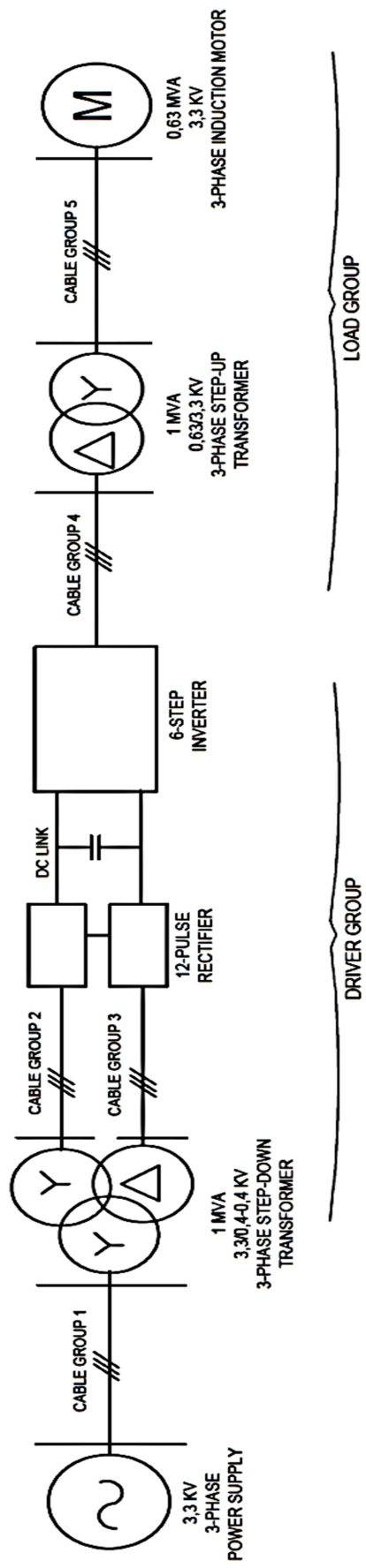


Figure 2.1 Single line diagram of the power system

cable trays, and conduits. Connections between the equipment are done by cables in these ways.

The main parts of the system analyzed are the driver group in the control center and the elements connected to its output. The group consisting of the transformer that shapes the output of the drive, the power cables providing the connection and the motor can be called the load group. In this system, the 3-phase power supply that supplies the system and the transformers that adjust the voltage level and are used for other specific purposes are close to the control center. The motor is in one of the production sections in the site. The single line diagram of the system is shown in Figure 2.1.

2.1 Components of the System

2.1.1 Driver Group

The driver is the system that supplies the motor with voltage of the required frequency and magnitude to enable the motor to function properly. The AC medium voltage six-step driver that used for this purpose consisting of 3 main parts; rectifier, dc link and inverter. A twelve pulse rectifier is converting the AC voltage to DC. The DC link provides the connection between the rectifier and the other part of the system and smooths the DC voltage ripple with the capacitor it contains. The three-phase inverter converts DC voltage back to AC and provides 3-phase voltage at desired frequency according to control type installed.

2.1.1.1 12-Pulse Rectifier

The 12-pulse rectifier is formed by connecting two 6-pulse bridge rectifiers in series, as shown in Figure 2.2. In addition, to ensure the 12-pulse structure, the connection of the rectifier groups to the source is made by a 3-winding transformer consisting of one primary winding and two secondary windings.

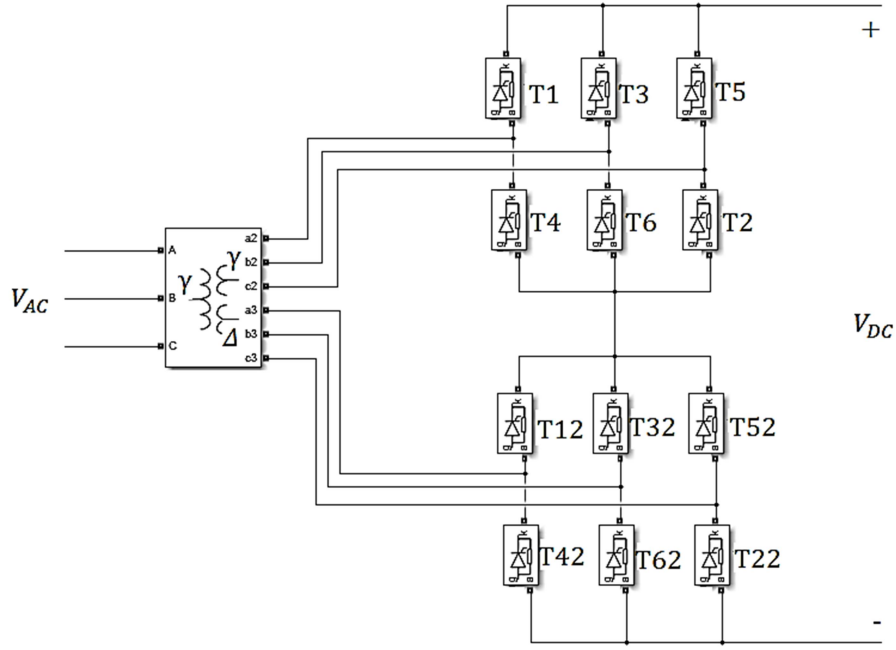


Figure 2.2 Structure of the 12-pulse rectifier

The voltage seen at the output of the first rectifier group corresponds to the secondary V_{ab} voltage when T_1 and T_6 are conducting, and to the secondary V_{ac} voltage when T_1 and T_2 are conducting, and to secondary V_{bc} voltage when T_3 and T_2 are conducting. In summary, the switches of the first rectifier are triggered as “ $T_1T_2, T_2T_3, T_3T_4, T_4T_5, T_5T_6, T_6T_1 \dots$ ” (Rashid, 2013) and the output voltage of the group is obtained as in Figure 2.3. Similarly, the trigger sequence of the second rectifier group respectively is “ $T_{12}T_{22}, T_{22}T_{32}, T_{32}T_{42}, T_{42}T_{52}, T_{52}T_{62}, T_{62}T_{12} \dots$ ” and the resulting output voltage of the group is also given in Figure 2.3. As shown in Figure 2.2, the transformer windings feeding one of the rectifier groups are connected in the form of wye-wye, while the windings feeding the other group are connected in the form of wye-delta. These connection forms result in a phase difference of 30 degrees between the output voltages of the rectifier groups. The output voltage of the 12-pulse rectifier is equal to the sum of the output voltages of these two rectifier groups and has a smoother output waveform thanks to the existing phase difference, as can be seen in Figure 2.3.

The average value of the DC output voltage of the 12-pulse rectifier can be expressed as equation (2.1) (Williams, 2006).

$$V_{dc} = V_1 + V_2 = \frac{6\sqrt{2}V_{LL}}{\pi N} \cos \alpha \quad (2.1)$$

where,

V_{LL} : Input line to line voltage

N : transformer turns ratio

α : the firing angle of semiconductor switches

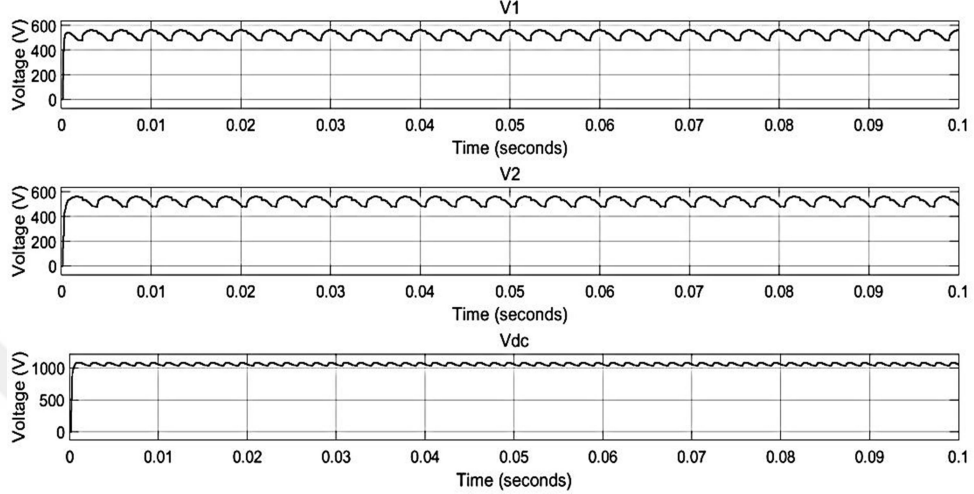


Figure 2.3 Output voltage waveforms of the rectifier

As can be seen from equation 1, if the alpha (α) angle increases, the output voltage decreases, if the alpha angle decreases, the output voltage increases and theoretically the maximum output voltage is obtained at 0 degree. Thus, by adjusting the alpha angle, the output of the rectifier can be controlled.

In theory, the value of the alpha angle can be between 0 degrees and 180 degrees. A converter operates as a rectifier and provides a positive DC output with alpha angle less than 90 degrees and it works as an inverter and gives a negative DC output with alpha angle greater than 90 degrees (Williams, 2006). However, there is a relationship between the time the thyristor remains in conduction, the overlap time and the ignition time, as shown in equation (2.2) (Mohan, Undeland & Robbins, 2003). Therefore, the alpha angle generally cannot reach 180 degrees.

$$\alpha + \mu + \gamma = 180^\circ \quad (2.2)$$

where,

μ : overlap angle

γ : ignition angle

The alpha angle can be set using either DC current control or DC voltage limitation control. However, in order to see the effects of resonance on the system more clearly, it was not preferred to keep the rectifier output at the desired level with a close loop control system in this thesis. The fixed alpha ($\alpha=0$) method was used to ensure the 12-pulse structure to operate in rectification mode and to obtain maximum output voltage instead.

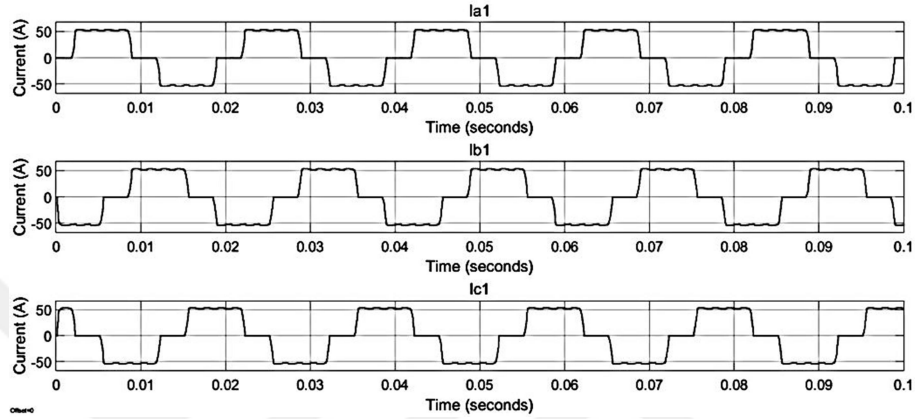


Figure 2.4 Input current of the first rectifier group

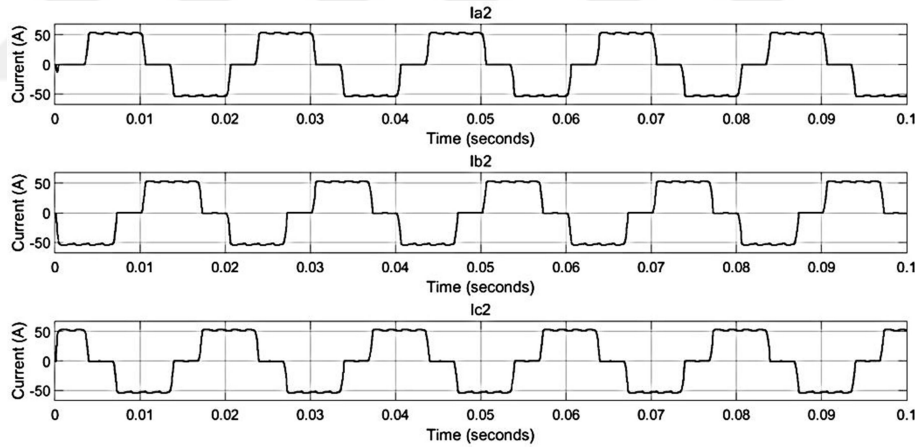


Figure 2.5 Input current of the second rectifier group

The currents of the lines connected to the arms of the first rectifier group are equal to " $I_{T1} - I_{T4}$ ", " $I_{T2} - I_{T6}$ ", and " $I_{T5} - I_{T2}$ " respectively, and the waveforms are as in Figure 2.4. The line currents of the second group are shown in Figure 2.5. In the 12 pulse rectifier, the input current is equal to the sum of the current magnitudes of these two groups transferred to the primary side, and the waveform is closer to the sine, as seen in Figure 2.6.

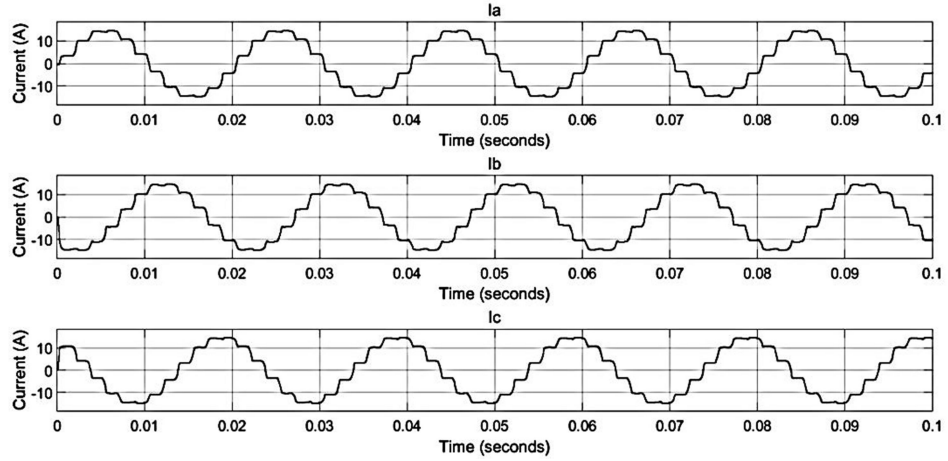


Figure 2.6 Input current of the 12-pulse rectifier group

Current harmonics at the source side can be estimated from formula (2.3) (Williams, 2006). When 12-pulse rectifier is used, there are not some important harmonics such as 5th and 7th harmonics in the drawn current. Therefore, this structure reduces the total harmonic distortion of current and is preferred because of this feature.

$$h = 12n \pm 1 \quad (2.3)$$

where,
 $n=1,2,3\dots$

2.1.1.2 DC Link

DC link provides a connection between rectifier and inverter and also it transfers power as irreversible. In order for the drive system to work more proper, it is desirable that the DC link voltage is more stable. Thus, smoothing capacitor is placed between the rectifier and the inverter to obtain a more smoothed DC link voltage waveform.

The rectifier output voltage is initially 0 V and then fluctuates as the waveform shown in Figure 2.3. When the capacitor is added to the system, the capacitor is charged while the output voltage of the rectifier increases, and then it releases the stored energy while the voltage decreases. Thus, the voltage variation is not sharp and the voltage waveform becomes smoothed as shown in Figure 2.7.

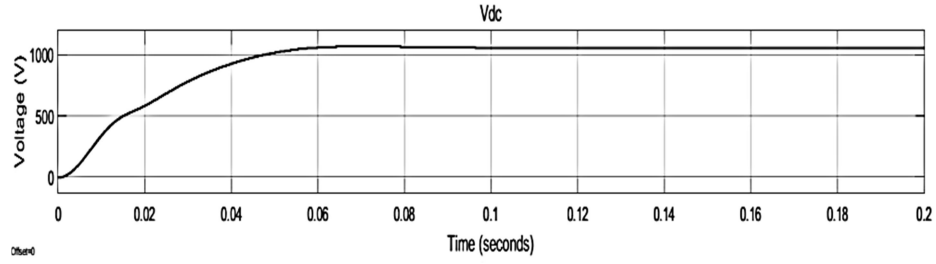


Figure 2.7 The waveform of the rectifier output voltage after using the capacitor

2.1.1.3 Six-Step (Square-wave) Inverter

The six-step inverter consists of 6 semiconductor switches (IGBT), and 6 diodes connected in parallel to them that to provide reactive power feedback (Williams, 2006), as shown in Figure 2.8. This is the main part that determines the output characteristic of the drive. In the preferred 120-degree conduction mode, the gate signals of the inverter are as shown in Figure 2.10. These waveforms can be obtained by converting the 180-degree conduction mode gate signals shown in Figure 2.13 with the logical circuit shown in Figure 2.9. In this mode, each inverter switch remains in conduction for 120 degrees and only two switches are conducting at the same time (Eyüp & Pillay, 1994).

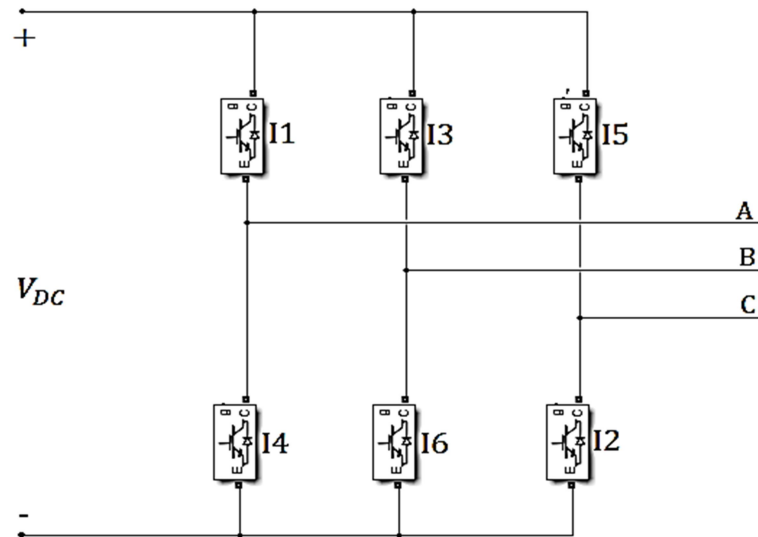


Figure 2.8 The structure of 6-step inverter

The switch groups in conduction change six times at 60-degree intervals over a period. The switching sequence is as "I6I1, I1I2, I2I3, I3I4, I4I5, I5I6, I6I1" (Rashid, 2013). In the mode, theoretically expected phase-neutral and phase-to-phase output

voltages are as shown in Figure 2.11 and 2.12, respectively. There is a range of 60 degrees between the switching moments of the switches in the same leg. In this range, the effect of EMF caused by inductive loads is seen on the terminal voltages of the associated phase (Eyüp et al., 1994). In case of loads with high power factor such as the motor, the output current of the inverter will be observed as discontinuous (Eyüp & Pillay, 1993). Thus, in such loads despite the switching mode, the output waveform will be as in the 180-degree conduction mode (Williams, 2006). In the 180 degree conduction mode, the phase-to-neutral voltage waveforms are as shown in Figure 2.14 and the phase-to-phase voltage waveforms as shown in Figure 2.15.

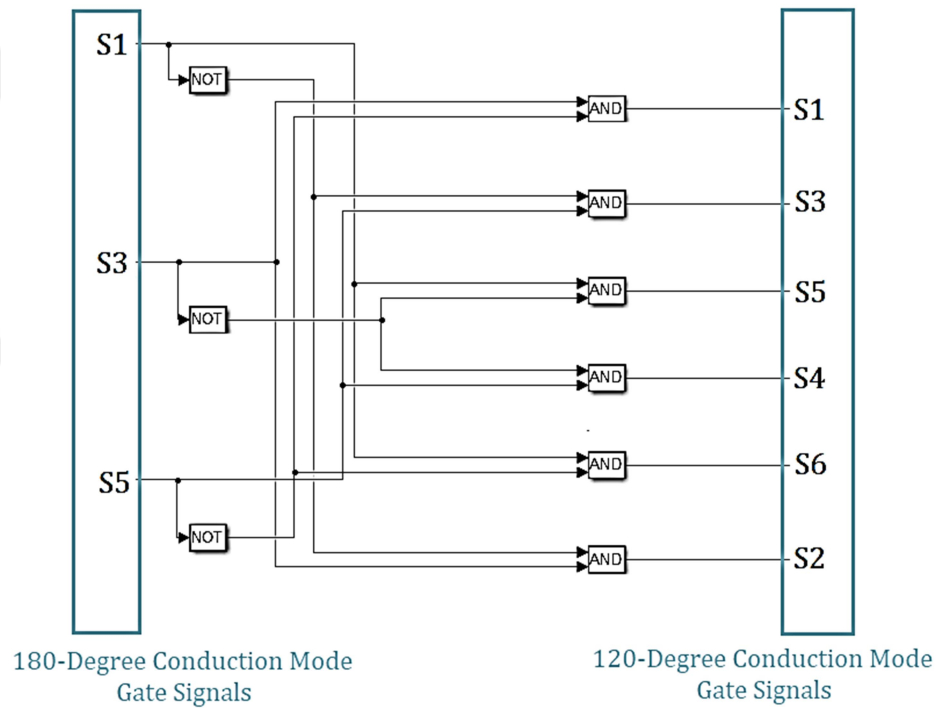


Figure 2.9 Logical transition circuit between 120-degree and 180-degree conduction modes

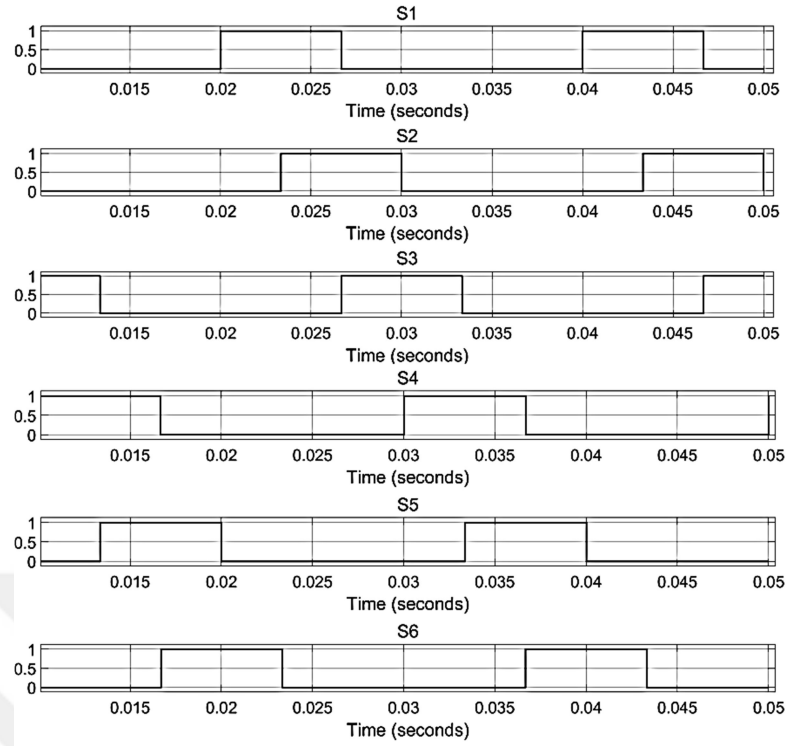


Figure 2.10 Gate signals in 120-degree conduction

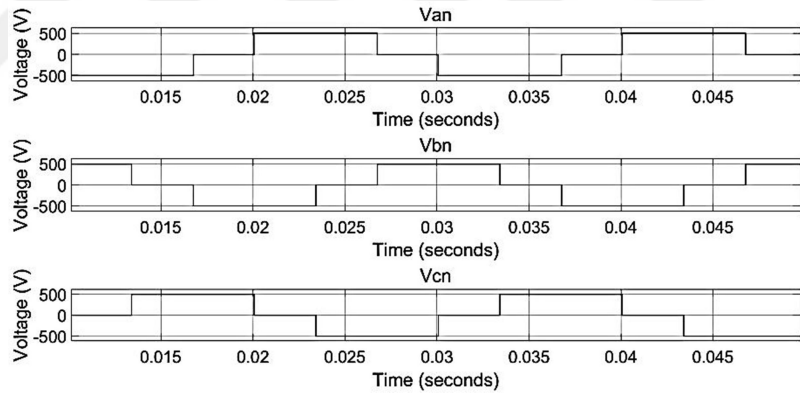


Figure 2.11 Phase-neutral in 120-degree conduction

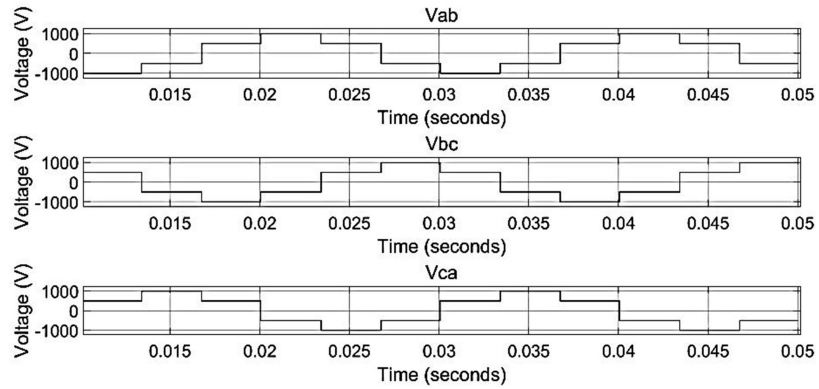


Figure 2.12 Phase-phase in 120-degree conduction

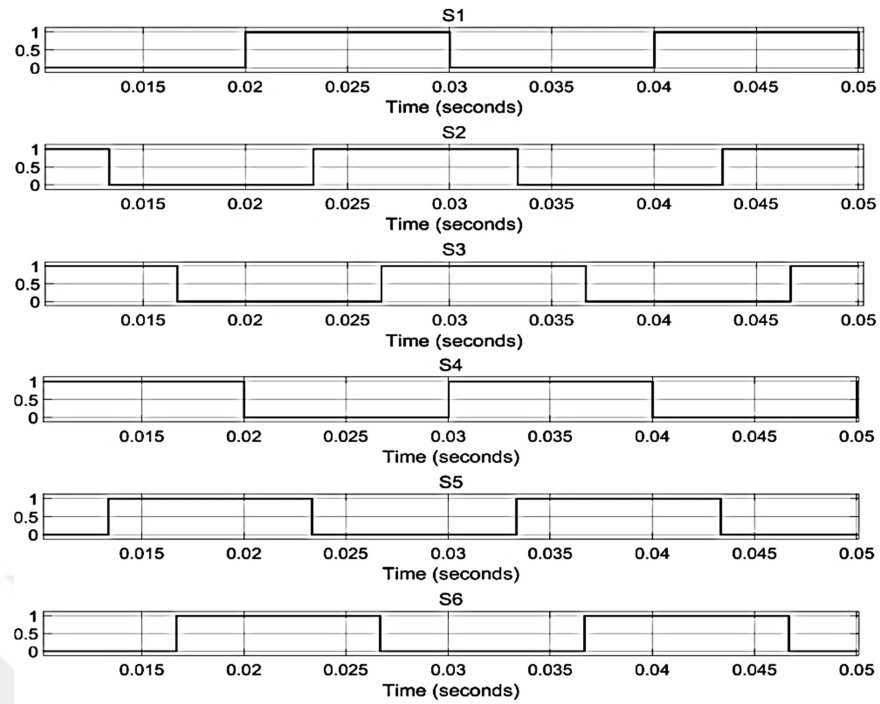


Figure 2.13 Gate signals in 180-degree conduction

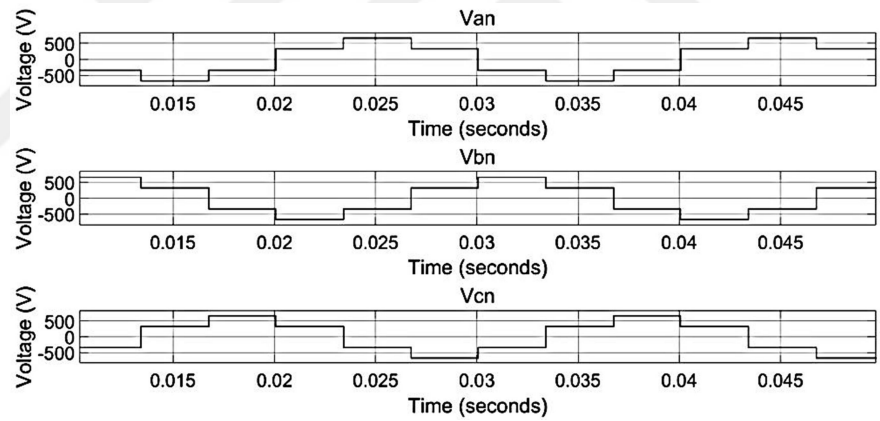


Figure 2.14 Phase-neutral in 180-degree conduction

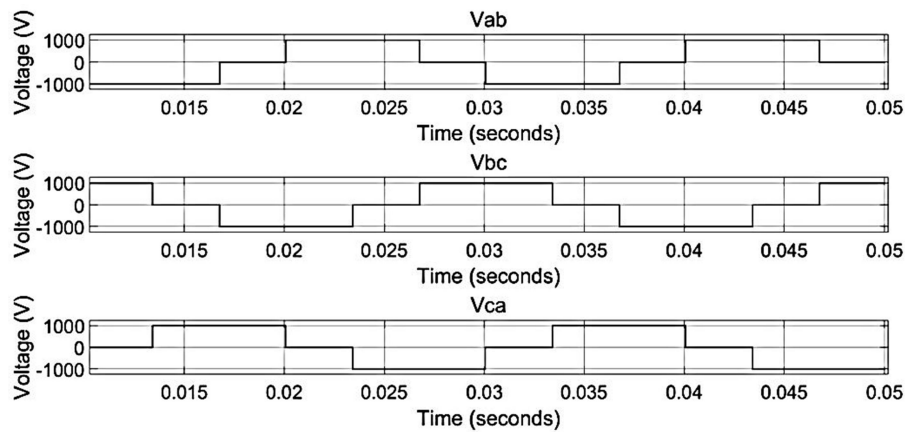


Figure 2.15 Phase-phase in 180-degree conduction

In inverter output voltage, the harmonics that may arise from the structure of the drive can be estimated by equation (2.4). (Williams, 2006). The harmonics that may be encountered in the inverter input are expressed by equation (2.5) due to 12-pulse structure of the rectifier.

$$h = 6n \pm 1 \quad (2.4)$$

$$h = 12n \quad (2.5)$$

Possible effects of harmonic components can be expressed by harmonic factor, distortion factor, and total harmonic distortion. Equation (2.6), equation (2.7) and equation (2.8) that expressing these factors are as follows (Williams, 2006).

$$\rho_n = \left| \frac{V_n}{V_1} \right| \quad (2.6)$$

$$\mu_n = \left| \frac{V_m}{nV_1} \right| \quad (2.7)$$

$$THD = \frac{\sqrt{\sum_{n \geq 2}^{\infty} \left(\frac{V_n}{V_1} \right)^2}}{V_1} \quad (2.8)$$

Variable frequency application is usually done using scalar control, vector control, direct torque control or intelligent control strategies (Sueker, 2005). Figure 2.16 shows the structure of the open loop scalar control block used in this system.

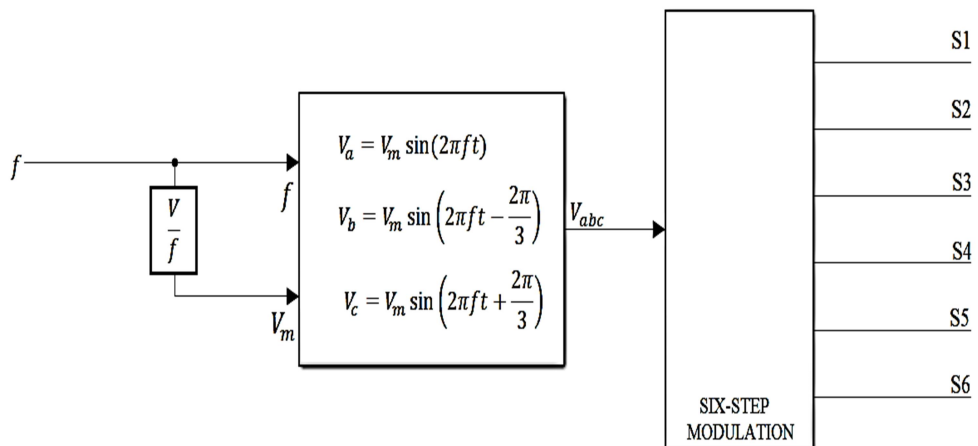


Figure 2.16 Scalar control

2.1.2 Load Group

2.1.2.1 Step-up Transformer

The transformer changes the voltage and current levels without changing the total power of the electricity. In this system, a three-phase step-up transformer is used to increase the level of inverter output voltage, and to shape the waveform. In this transformer which has a primary and secondary winding, winding connections are made as delta-wye (Takacs, 2009). The secondary voltage is greater than the primary voltage and also the number of turns of the secondary winding is greater than the number of turns of the primary winding. At the same time, the current magnitude is less in the secondary winding.

The transformer operates according to Faraday's Law and converts electrical energy first to magnetic energy, then back to electrical energy. When the current is applied to the primary winding, a magnetic field is formed and it links the secondary winding. The voltage is also induced in the secondary winding and the current begins to flow when the load is connected to the secondary terminals.

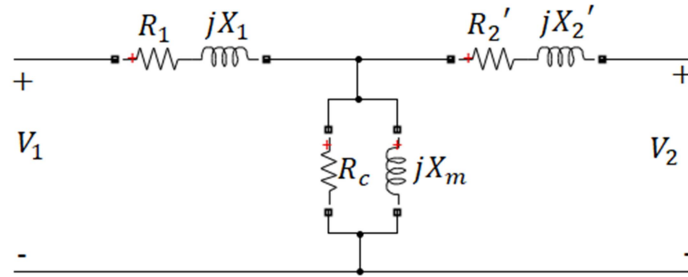


Figure 2.17 The equivalent circuit of the transformer referred to primary side

Where,

R_1 : Primary winding resistance (Ω)

X_1 : Primary winding leakage reactance (Ω)

R_2 : Secondary winding resistance (Ω)

X_2 : Secondary winding leakage reactance (Ω)

R_c : Core-loss resistance (Ω)

X_m : Magnetizing reactance (Ω)

The single-phase equivalent circuit of a transformer, referred to the primary side, is as in Figure 2.17 (Saadat, 2010). The heat of the conductors increases with the effect of current and copper losses occur. These losses are represented as winding

resistances(R_1 , R_2) in the equivalent circuit. The magnetic flux can not circulate as a whole through the core, some of it leaks out of ferromagnetic core. These leaks are represented by leakage reactances (X_1 , X_2). The magnetic field to be generated for magnetization is expressed through magnetization reactance (X_m). Core losses due to hysteresis and eddy currents are represented as resistance(R_C) associated magnetization branch. Furthermore, the equivalent circuit can be transformed into the state of Figure 2.18, by omitting the magnetizing branch (Saadat, 2010).

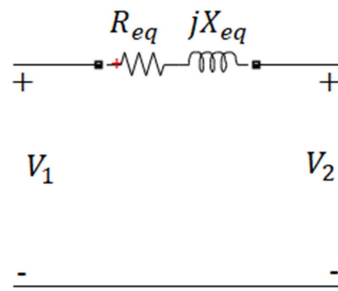


Figure 2.18 Simplified equivalent circuit of the transformer

2.1.2.2 The Power Cables

The cable provides an electrical connection between the equipment of the system and the transmission of electrical power. The 3-phase AC power cables used in these systems must be resistant to high temperatures, mechanical and chemical stresses from the environment. The cables are selected according to the rated voltage level, conductor material and insulation material (Takacs, 2009).

Copper or aluminum are generally used as conductors. Copper is a more expensive and heavier material compared to aluminum. However, the conductivity is better and it can provide the use of cables with a lower cross-section in these facilities where the installation is made with pipes. PVC (thermoplastic) and XLPE (crosslinked polyethylene) are used as insulation material. XLPE is more insensitive to temperature and chemical influences than PVC and is not as rigid and brittle as PVC. Therefore, XLPE insulated, three-cores, copper conductor, medium voltage cable (or 3 pcs single-core cables) may be preferred in this system. The cables may have a round or flat construction.

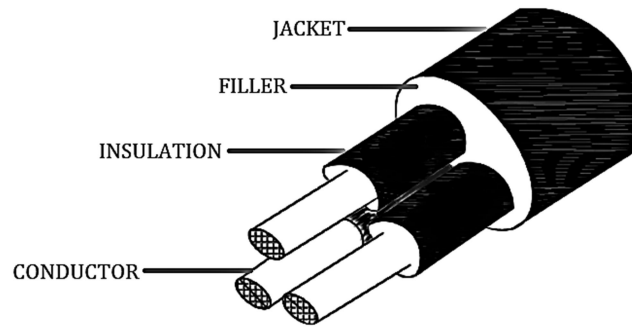


Figure 2.19 Structure of the power cable

The cable shown in Figure 2.19 is basically composed of the conductor, insulating sheath, filler material, and jacket. The conductor is the main part of the cable and carries the electricity. It can consist of a solid wire or multiple wires that twisted and compressed. The element that provides insulation and separates the phases is called the insulating sheath. By insulating conductors, cores are formed. In order to fill the gaps between the formed cores and to obtain the desired surface shape, common filler or common sheath made of materials such as cotton, synthetic wool yarn, rubber, thermoplastic, is used. In some cables, the screen may be wound onto this common sheath to limit the electric field. In addition, steel armor can be used to mechanically protect the cable as the voltage level increases or the ambient conditions get harder. However, on the outermost surface, there is an outer sheath(jacket) surrounding all these components of the cable.

These cables can be modeled as in Figure 2.20 (Cataliotti, Daidone, Sanacore & Tinè, 2008).

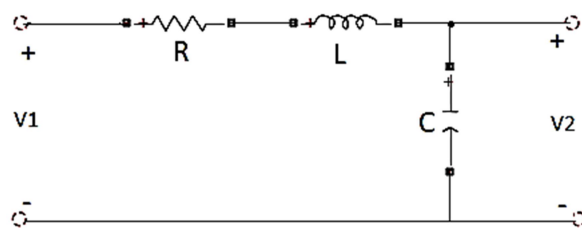


Figure 2.20 Simplified power cable equivalent circuit

The DC resistance (R) is the cable parameter resulting from the nature of the cable conductor, causing a voltage drop and active power loss. As seen in equation (2.9), its magnitude is related to the cross-section and length of the conductor (Thue, 2003).

The effective resistance is, in fact, AC resistance and differs from DC resistance. This difference caused by spirality effect, thermal effect, proximity effect and skin effect, becomes more and more evident especially as frequency increases. But this ratio can be neglected in normal operating conditions and AC resistance can be assumed to equal to DC resistance.

$$R_{dc} = 1000 \times \frac{\rho}{A} \quad (2.9)$$

where

ρ : resistivity of metal in ohms per circular mil foot

A : conductor area in circular mils

The inductance (L) of the cable is expressed in formula (2.10) and its value depends on the number of phases, the conductor diameters, the arrangement of the conductors and the distance between the conductors (Thue, 2003).

$$L = 0.1404 \log_{10} \frac{GMD}{GMR} \times 10^{-3} \quad (2.10)$$

where

GMD : geometric mean distance between conductors in inches

GMR : geometric Radius of conductors in inches

The conductors placed against each other show capacitive properties with the effect of components which have a dielectric character between them. This creates a charge on the conductors. The ratio of the electrical charge to the potential of the conductor is called capacity. The capacity value of the cable (C) is expressed by formula (2.11) (Thue, 2003).

$$C = \frac{\epsilon}{2 \log_e \frac{D}{d}} \quad (2.11)$$

where

ϵ : dielectric constant of the insulating material

D : outer diameter of the insulation

d : inside diameter of the insulation

2.1.2.3 The Induction Motor

The motor where the frequency of the rotating magnetic field formed by the stator is not the same as the rotational frequency of the rotor is called asynchronous motor, i.e. induction motor. While the rotating magnetic field speed depends on the motor supply and the number of poles of the motor, the rotational speed of the rotor is also related to the load. As the load increases the rotor speed decreases, as the load decreases the rotor speed increases and it reaches its highest level in idle. Asynchronous motors are divided into two types as rotor structure, squirrel cage type and wound type induction motor. In this system, 2 pole squirrel cage induction motor is used. In the squirrel cage motor, the conductor rods are placed in the rotor grooves and these rods are short-circuited on both sides. The rods placed diagonally ensure that the harmonics are less and the motor runs silently. Since both sides are short-circuited, this type of rotor has no outlet to the connection box. However, this type of motor does not have brushes and hence have a simpler structure, does not require much maintenance.

The induction motor consists of two main parts; the stator and the rotor. The stator is the stationary part of the motor and helps to create a rotating magnetic field. The stator structures of all types of the induction motors are completely identical except for the connection of the three-phase windings placed in the stator grooves. The winding ends are connected as star or delta in the connection box on the motor body and the motor is supplied from here. The rotor is the rotating part of the motor. In its grooves, there are conductive metal rods or windings. The stator and the rotor are located in a housing i.e. a body. The body is mounted on a pedestal where the motor is to be used with its feet. On the body, there is a terminal box where the motor electrical connections are done. In addition, there are other parts such as a fan for cooling the motor and a roller for comfortable rotation of the rotor.

$$n_s = 120 \times \frac{f}{p} \quad (2.12)$$

The rotating field speed of the stator is as in equation (2.12). The magnitude of the stator and rotor voltages of the machine is related to leakage flux reactances, winding resistances and magnetization reactance. In addition, the rotor angular

velocity is an effective electrical parameter. Voltage connections can be expressed as a function of currents, as in equation (2.13) (Krause, Wasynczuk & Sudhoff, 1995).

$$\begin{bmatrix} V_{qs} \\ V_{ds} \\ V_{qr}' \\ V_{dr}' \end{bmatrix} = \begin{bmatrix} r_s + \frac{p}{\omega_b} X_{ss} & \frac{\omega}{\omega_b} X_{ss} & \frac{p}{\omega_b} X_M & \frac{\omega}{\omega_b} X_M \\ -\frac{\omega}{\omega_b} X_{ss} & r_s + \frac{p}{\omega_b} X_{ss} & -\frac{\omega}{\omega_b} X_M & \frac{p}{\omega_b} X_M \\ \frac{p}{\omega_b} X_M & (\frac{\omega - \omega_r}{\omega_b}) X_M & r_r' + \frac{p}{\omega_b} X_{rr}' & (\frac{\omega - \omega_r}{\omega_b}) X_{rr}' \\ -(\frac{\omega - \omega_r}{\omega_b}) X_M & \frac{p}{\omega_b} X_M & -(\frac{\omega - \omega_r}{\omega_b}) X_{rr}' & r_r' + \frac{p}{\omega_b} X_{rr}' \end{bmatrix} \begin{bmatrix} i_{qs} \\ i_{ds} \\ i_{qr}' \\ i_{dr}' \end{bmatrix} \quad (2.13)$$

In order for the machine to function as a motor, the electromagnetic torque value must be positive. The torque generated by the asynchronous machine is given in equation (2.14) (Krause et al., 1995).

$$T_e = \left(\frac{3}{2}\right) \left(\frac{P}{2}\right) M(i_{qs}i_{dr}' - i_{ds}i_{qr}') \quad (2.14)$$

The leakage reactances, resistances and magnetization reactance of the machine can be shown in the single phase approximate equivalent circuit that appears in the steady state, as in Figure 2.21 (Diyoke, Okeke & Aniagwu, 2016).

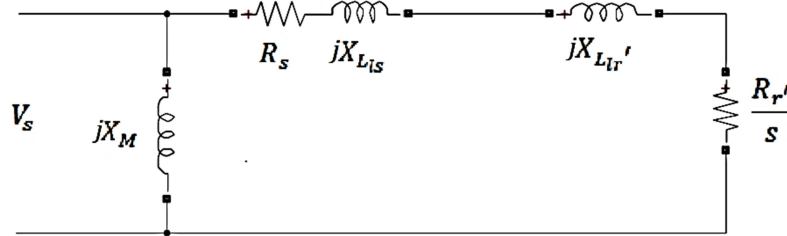


Figure 2.21 Simplified equivalent circuit of the induction motor

Where,

X_{Ls} : Stator leakage reactance

X_{Lr}' : Rotor leakage reactance

R_s : Stator resistance

R_r' : Rotor resistance

X_M : Magnetization reactance

The critical slip at which the maximum torque occurs can be calculated using formula (2.15).

$$s_{max} = \frac{R_r'}{\left[R_s^2 + (X_s + X_r')^2\right]^{\frac{1}{2}}} \quad (2.15)$$

2.2 Per-unit Conversion for the System Parameters

The analysis with per-unit values allows obtaining information that can be interpreted about the situations that may be encountered even when the system is designed at a different voltage, current, and power levels. In addition, conversion to per-unit values simplifies the system and reduces the likelihood of errors. Therefore, in order to make a more comprehensive evaluation, the actual values were converted to per unit values and computer simulations were performed using these values.

The DC link separates the system into two separate AC grids. By considering this case and the voltage levels of the transformers, the system can be divided into four zones. The identified zones are shown in Figure 2.22. A common base power value is selected for the entire system and voltage base values are determined according to these zones. The power base can be expressed by formula (2.17) (Akpınar et al., 1993). Base impedance, base inductance and base capacitance values can be determined by using formulas (2.18), (2.19) and (2.20) respectively according to the determined base power and voltage values (Krause et al., 1995).

$$S_{BASE} = 3V_{BASE}I_{BASE} \quad (2.17)$$

$$Z_{BASE} = \frac{3V_{BASE}^2}{S_{BASE}} \quad (2.18)$$

$$L_{BASE} = \frac{Z_{BASE}}{2\pi f} \quad (2.19)$$

$$C_{BASE} = \frac{1}{Z_{BASE} \times 2\pi} \quad (2.20)$$

For equipment with rotating components such as motors, the base speed must also be determined. The load torque can be calculated according to formula (2.21) (Krause et al., 1995). In Per-unit systems, Inertia constant (H) is used instead of the Moment of inertia (J) in SI. Inertia constant (H) is expressed in equation (2.22) (Krause et al., 1995).

$$T_{BASE} = \frac{P_{BASE}}{\left(\frac{2}{p}\right)\omega_{BASE}} \quad (2.21)$$

$$H = \frac{\frac{1}{2} \times J \times \omega^2}{P_n} \quad (2.22)$$

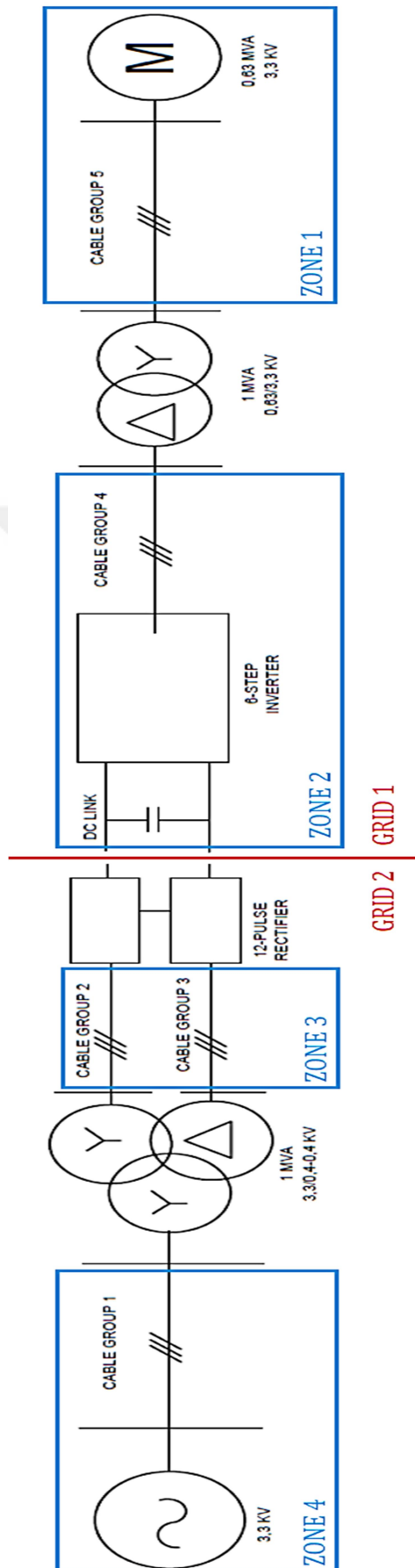


Figure 2.22 Zones of the system

Table 2.1 Electrical parameters of cables (per kilometer)

Cable Group No	DC Resistance (Ω/km)	Inductance (H/km)	Capacitance (F/km)	Length (km)
1	0.387	0.351×10^{-3}	0.318×10^{-6}	0.1
2	0.0754	0.284×10^{-3}	0.587×10^{-6}	0.1
3	0.0754	0.284×10^{-3}	0.587×10^{-6}	0.1
4	0.0283	0.264×10^{-3}	0.739×10^{-6}	0.02
5	0.387	0.351×10^{-3}	0.318×10^{-6}	5

Table 2.2 Electrical parameters of three-winding step-down transformer

Nominal Power (MVA)	Type of Connection	Winding 1 Parameters (Primer Side)			Winding 2 Parameters (Seconder Side)			Winding 3 Parameters (Seconder Side)			Magnetization Branch Parameters	
		Ph-Ph Voltage (KV)	R1 (Ω)	L1 (H)	Ph-Ph Voltage (KV)	R2 (Ω)	L2 (H)	Ph-Ph Voltage (KV)	R3 (Ω)	L3 (H)	Rm (Ω)	Lm (H)
1	WYE-WYE, DELTA	3.3	6.534×10^{-3}	1.3866×10^{-3}	0.4	9.6×10^{-5}	2.0372×10^{-5}	0.4	2.88×10^{-4}	6.1115×10^{-5}	5445	17.332

Table 2.3 Electrical parameters of step-up transformer

Nominal Power (MVA)	Type of Connection	Winding 1 Parameters (Primer Side)			Winding 2 Parameters (Seconder Side)			Magnetization Branch Parameters	
		Ph-Ph Voltage (KV)	R1 (Ω)	L1 (H)	Ph-Ph Voltage (KV)	R2 (Ω)	L2 (H)	Rm (Ω)	Lm (H)
1	DELTA-WYE	0.63	1.1907×10^{-5}	7.5802×10^{-5}	3.3	1.089×10^{-4}	6.9328×10^{-4}	119.07	0.3790

Table 2.4 Electrical parameters of induction motor

Nominal Power (MVA)	Voltage (Ph-Ph) (KV)	Stator Resistance Rs (Ω)	Stator Inductance Lls (H)	Rotor Resistance Rr' (Ω)	Rotor Inductance Llr' (H)	Mutual inductance Lm (H)	Inertia constant J ($kg.m^2$)	Pole Pairs p	Load torque T_L (Nm)
0.63	3.3	0.973	7.7445×10^{-3}	1.238	9.5111×10^{-3}	0.1749	2.6	1	1000

Table 2.5 Value of DC link capacitance

Smoothing Capacitance (F)
0.05

Table 2.6 Electrical parameter of three-phase voltage source

Voltage (phase-to-phase) (KV)	Source Resistance (Ω)	Source Inductance (H)
3.3	0.8929	16.58×10^{-3}

As stated in formula (2.23), the per-unit values of the parameters such as torque, impedance, inductance and capacitance are calculated by dividing the actual values by the specified base values. The per-unit impedance values given by the manufacturers are generally based on the nominal power of the equipment. However, to convert the entire system to per-unit, all components in the system must be converted according to the base power value. Thus, these impedances are expressed on a common base using formula (2.24) (Saadat, 2010).

$$Value_{pu} = \frac{Value_{actual}}{Value_{BASE}} \quad (2.23)$$

$$Z_{pu}^{new} = Z_{pu}^{old} \times \frac{S_{base}^{new}}{S_{base}^{old}} \times \left(\frac{V_{base}^{old}}{V_{base}^{new}} \right)^2 \quad (2.24)$$

The rated values and electrical parameters of the components of the system are given in tables 2.1, 2.2, 2.3, 2.4, 2.5 and 2.6. These values were converted to per-unit as follows using the given formulas.

Zone 1:

$$S_B = 1 \text{ MVA}$$

$$V_{B1} = 3.3 \text{ kV}$$

According to formulas (2.18), (2.19) and (2.20), the base values of the Zone 1 are as follows.

$$Z_{B1} = \frac{V_{B1}^2}{S_B} = \frac{(3.3 \times 10^3)^2}{\frac{1 \times 10^6}{3}} = 32.67 \Omega$$

$$L_{B1} = \frac{Z_{B1}}{2\pi f} = \frac{32.67}{2 \times \pi \times 50} = 0.1039 \text{ H}$$

$$C_{B1} = \frac{1}{Z_{B1} \times 2\pi f} = \frac{1}{32.67 \times 2 \times \pi \times 50} = 9.7432 \times 10^{-5} \text{ F}$$

Cable Group 5:

According to formula (2.23), the per unit values of the cables in group 5 are as follows.

$$R5_{pu} = \frac{0.387}{32.67} = 0.0118 \text{ pu}$$

$$L5_{pu} = \frac{0.351 \times 10^{-3}}{0.1039} = 3.3782 \times 10^{-3} \text{ pu}$$

$$C5_{pu} = \frac{0.318 \times 10^{-6}}{9.7432 \times 10^{-5}} = 3.2638 \times 10^{-3} \text{ pu}$$

Motor:

$$\omega_{base} = 314.16 \text{ rad/s}$$

According to the equation (2.18), the impedance base at the rated values of the motor as follows.

$$Z_{base(m)} = \frac{3.3^2}{0.63} = 17.2857 \Omega$$

According to the equation (2.23), the per-unit values at the rated values as follows.

$$r_{s_{pu}} = \frac{0.973}{17.2857} = 0.0563 \text{ pu}$$

$$Ll_{s_{pu}} = \frac{7.7445 \times 10^{-3}}{\frac{17.2857}{2\pi f}} = 0.141 \text{ pu}$$

$$r_{r'_{pu}} = \frac{1.238}{17.2857} = 0.07162 \text{ pu}$$

$$Ll_{r'_{pu}} = \frac{9.5111 \times 10^{-3}}{\frac{17.2857}{2\pi f}} = 0.173 \text{ pu}$$

$$L_{m_{pu}} = \frac{0.1749}{\frac{17.2857}{2\pi f}} = 3.18 \text{ pu}$$

According to formula (2.21) and (2.23), respectively base torque and per-unit torque values are as follows.

$$T_{base} = \frac{P_{base}}{w_{base}} = \frac{0.63 \times 10^6}{\left(\frac{2}{\pi}\right) \times 314} = 2006.369 \text{ N.m}$$

$$T_L = \frac{1000}{2006.369} = 0.498 \text{ pu}$$

According to the equation (2.24), the per unit values of the motor are expressed on the common base as follows.

$$r_{s_{pu}}^{new} = 0.0563 \times \frac{1}{0.63} \times \left(\frac{3.3}{3.3}\right)^2 = 0.0894 \text{ pu}$$

$$Ll_{s_{pu}}^{new} = 0.141 \times \frac{1}{0.63} = 0.2238 \text{ pu}$$

$$r_{r'_{pu}}^{new} = 0.07162 \times \frac{1}{0.63} = 0.1137 \text{ pu}$$

$$Ll_{r'_{pu}}^{new} = 0.173 \times \frac{1}{0.63} = 0.2746 \text{ pu}$$

$$L_{m_{pu}}^{new} = 3.18 \times \frac{1}{0.63} = 5.0476 \text{ pu}$$

Inertia constant according to equation (2.22) as follows.

$$H = \frac{\frac{1}{2} \times 2.6 \times 314.16^2}{630 \times 10^3} = 0.20366$$

Base and per-unit torque in new base according to equation (2.21) and (2.23) respectively as follows.

$$T_{base} = \frac{P_{base}}{w_{base}} = \frac{1 \times 10^6}{314} = 3184.713 \text{ N.m}$$

$$T_L = \frac{1000}{3184.713} = 0.314 \text{ pu}$$

Step-up Transformer:

The base and per-unit values of the transformer are as follows considering the connection types.

In secondary winding (λ);

$$Z_{B1\lambda} = \frac{V_{B1\lambda}^2}{S_B} = \frac{\left(\frac{3.3 \times 10^3}{\sqrt{3}}\right)^2}{\frac{1 \times 10^6}{3}} = 10.89 \Omega$$

$$r2_{pu} = \frac{1.089 \times 10^{-4}}{10.89} = 1 \times 10^{-5} \text{ pu}$$

$$l2_{pu} = \frac{6.9328 \times 10^{-4}}{\frac{10.89}{2\pi f}} = 0.02 \text{ pu}$$

In primary winding (Δ);

$$Z_{B2\Delta} = \frac{V_{B2\Delta}^2}{S_B} = \frac{(0.63 \times 10^3)^2}{\frac{1 \times 10^6}{3}} = 1.1907 \Omega$$

$$r1_{pu} = \frac{1.1907 \times 10^{-5}}{1.1907} = 1 \times 10^{-5} \text{ pu}$$

$$l1_{pu} = \frac{7.5802 \times 10^{-5}}{\frac{1.1907}{2\pi f}} = 0.02 \text{ pu}$$

$$rm_{pu} = \frac{119.07}{1.1907} = 100 \text{ pu}$$

$$lm_{pu} = \frac{0.3790}{\frac{1.1907}{2\pi f}} = 100 \text{ pu}$$

Zone 2:

$$V_{B2} = 3.3 \left(\frac{0.63}{3.3} \right) = 0.63 \text{ kV}$$

According to formulas (2.18), (2.19) and (2.20), the base values of the Zone 2 are as follows.

$$Z_{B2} = \frac{V_{B2}^2}{S_B} = \frac{(0.63 \times 10^3)^2}{\frac{1 \times 10^6}{3}} = 1.1907 \Omega$$

$$L_{B2} = \frac{Z_{B2}}{2\pi f} = \frac{1.1907}{2 \times \pi \times 50} = 3.7901 \times 10^{-3} \text{ H}$$

$$C_{B2} = \frac{1}{Z_{B2} \times 2\pi f} = \frac{1}{1.1907 \times 2 \times \pi \times 50} = 2.6733 \times 10^{-3} \text{ F}$$

Cable group 4:

According to formula (2.23), the per unit values of the cables in group 4 are as follows.

$$R4_{pu} = \frac{0.0283}{1.1907} = 0.0238 \text{ pu}$$

$$L4_{pu} = \frac{0.264 \times 10^{-3}}{3.7901 \times 10^{-3}} = 0.0697 \text{ pu}$$

$$C4_{pu} = \frac{0.739 \times 10^{-6}}{2.6733 \times 10^{-3}} = 2.764 \times 10^{-4} \text{ pu}$$

DC link capacitor:

To ensure integrity in the system, the DC capacitor is also referred to as per-unit.

$$C_{S_{pu}} = \frac{0,05}{2.6733 \times 10^{-3}} = 18.7035 \text{ pu}$$

Zone 3:

$$V_{B3} = 0.4 \text{ kV}$$

According to formulas (2.18), (2.19) and (2.20), the base values of the Zone 3 are as follows.

$$Z_{B3} = \frac{V_{B3}^2}{S_B} = \frac{(0.4 \times 10^3)^2}{\frac{1 \times 10^6}{3}} = 0.48 \Omega$$

$$L_{B3} = \frac{Z_{B3}}{2\pi f} = \frac{0.48}{2 \times \pi \times 50} = 1.5279 \times 10^{-3} \text{ H}$$

$$C_{B3} = \frac{1}{Z_{B3} \times 2\pi f} = \frac{1}{0.48 \times 2 \times \pi \times 50} = 6.6315 \times 10^{-3} \text{ F}$$

Cable group 2 and 3:

According to formula (2.23), the per unit values of the cables in group 2 and group 3 are as follows.

$$R2_{pu} = \frac{0.0754}{0.48} = 0.1571 \text{ pu}$$

$$L2_{pu} = \frac{0.284 \times 10^{-3}}{1.5279 \times 10^{-3}} = 0.1859 \text{ pu}$$

$$C2_{pu} = \frac{0.587 \times 10^{-6}}{6.6315 \times 10^{-3}} = 8.852 \times 10^{-5} \text{ pu}$$

$$R3_{pu} = 0.1571 \text{ pu}$$

$$L3_{pu} = 0.1859 \text{ pu}$$

$$C3_{pu} = 8.852 \times 10^{-5} \text{ pu}$$

Step-down Transformer:

The base and per-unit values of the transformer are as follows considering the connection types.

In secondary winding 1 (λ);

$$Z_{B3\lambda} = \frac{V_{B3\lambda}^2}{S_B} = \frac{\left(\frac{0.4 \times 10^3}{\sqrt{3}}\right)^2}{\frac{1 \times 10^6}{3}} = 0.16 \Omega$$

$$r_{2\lambda_{pu}} = \frac{9.6 \times 10^{-5}}{0.16} = 0.0006 \text{ pu}$$

$$l_{2\lambda_{pu}} = \frac{2.0372 \times 10^{-5}}{\frac{0.16}{2\pi f}} = 0.04 \text{ pu}$$

In secondary winding 2 (Δ);

$$Z_{B3\Delta} = \frac{V_{B3\Delta}^2}{S_B} = \frac{(0.4 \times 10^3)^2}{\frac{1 \times 10^6}{3}} = 0.48 \Omega$$

$$r_{2\Delta_{pu}} = \frac{2.88 \times 10^{-4}}{0.48} = 0.0006 \text{ pu}$$

$$l_{2\Delta_{pu}} = \frac{6.1115 \times 10^{-5}}{\frac{0.48}{2\pi f}} = 0.04 \text{ pu}$$

In primary winding (λ);

$$Z_{B4\lambda} = \frac{V_{B4\lambda}^2}{S_B} = \frac{\left(\frac{3.3 \times 10^3}{\sqrt{3}}\right)^2}{\frac{1 \times 10^6}{3}} = 10.89 \Omega$$

$$r_{1_{pu}} = \frac{6.534 \times 10^{-3}}{10.89} = 0.0006 \text{ pu}$$

$$l1_{pu} = \frac{1.3866 \times 10^{-3}}{\frac{10.89}{2\pi f}} = 0.04 \text{ pu}$$

$$rm_{pu} = \frac{5445}{10.89} = 500 \text{ pu}$$

$$lm_{pu} = \frac{17.332}{\frac{10.89}{2\pi f}} = 500 \text{ pu}$$

Zone 4:

$$V_{B4} = 0.4 \left(\frac{3.3}{0.4} \right) = 3.3 \text{ kV}$$

According to formulas (2.18), (2.19) and (2.20), the base values of the Zone 4 are as follows.

$$Z_{B4} = \frac{V_{B4}^2}{S_B} = \frac{(3.3 \times 10^3)^2}{\frac{1 \times 10^6}{3}} = 32.67 \Omega$$

$$L_{B4} = \frac{Z_{B4}}{2\pi f} = \frac{32.67}{2 \times \pi \times 50} = 0.1039 \text{ H}$$

$$C_{B4} = \frac{1}{Z_{B4} \times 2\pi f} = \frac{1}{32.67 \times 2 \times \pi \times 50} = 9.7432 \times 10^{-5} \text{ F}$$

Cable group 1:

According to formula (2.23), the per unit values of the cables in group 1 are as follows.

$$R1_{pu} = \frac{0.387}{32.67} = 0.0118 \text{ pu}$$

$$L1_{pu} = \frac{0.351 \times 10^{-3}}{0.1039} = 3.3782 \times 10^{-3} \text{ pu}$$

$$C1_{pu} = \frac{0.318 \times 10^{-6}}{9.7432 \times 10^{-5}} = 3.2638 \times 10^{-3} \text{ pu}$$

Source:

The base and per-unit values of the source are as follows considering the connection types.

$$Z_{Bs\lambda} = \frac{V_{Bs\lambda}^2}{S_B} = \frac{\left(\frac{3.3 \times 10^3}{\sqrt{3}}\right)^2}{\frac{1 \times 10^6}{3}} = 10.89 \Omega$$

$$r_{s_{pu}} = \frac{0.8929}{10.89} = 0.082 \text{ pu}$$

$$l_{s_{pu}} = \frac{16.58 \times 10^{-3}}{\frac{10.89}{2\pi f}} = 0.4783 \text{ pu}$$

All calculated per-unit values are given in the following tables. These values are used in the simulation with the Matlab commands given in Appendix 1.

Table 2.7 Per-unit electrical parameters of cables (per kilometer)

Line No	Resistance (pu)	Inductance (pu)	Capacitance (pu)	Length (km)
1	0.0118	3.3782×10^{-3}	3.2638×10^{-3}	0.1
2	0.1571	0.1859	8.852×10^{-5}	0.1
3	0.1571	0.1859	8.852×10^{-5}	0.1
4	0.0238	0.0697	2.764×10^{-4}	0.02
5	0.0118	3.3782×10^{-3}	3.2638×10^{-3}	5

Table 2.8 Per-unit electrical parameters of three-winding step-down transformer

Nominal Power (MVA)	Type of Connection	Winding 1 Parameters (Primer Side)			Winding 2 Parameters (Seconder Side)			Winding 3 Parameters (Seconder Side)			Magnetization Branch Parameters	
		Ph-Ph Voltage KV	R1 pu	L1 pu	Ph-Ph Voltage KV	R2 pu	L2 pu	Ph-Ph Voltage KV	R3 pu	L3 pu	Rm (pu)	Lm (pu)
1	WYE-WYE, DELTA	3.3	0.0006	0.04	0.4	0.0006	0.04	0.4	0.0006	0.04	500	500

Table 2.9 Per-unit electrical parameters of step-up transformer

Nominal Power (MVA)	Type of Connection	Winding 1 Parameters (Primer Side)			Winding 2 Parameters (Primer Side)			Magnetization Branch Parameters	
		Ph-Ph Voltage KV	R1 pu	L1 pu	Ph-Ph Voltage KV	R2 pu	L2 pu	Lm (pu)	Rm (pu)
1	DELTA-WYE	0.63	1.10^{-5}	0.02	3.3	1.10^{-5}	0.02	100	100

Table 2.10 Per-unit electrical parameters of induction motor

Nominal power MVA	Voltage (line-line) KV	Stator Resistance Rs pu	Stator Inductance Lls pu	Rotor Resistance Rr' pu	Rotor Inductance Llr' pu	Mutual inductance Lm (pu)	Inertia constant H	Pole Pairs p	Load Torque (pu)
0.63	3.3	0.0563	0.141	0.07162	0.173	3.18	0.2037	1	0.498
1	3.3	0.0894	0.2238	0.1137	0.2746	5.0476	0.2037	1	0.314

Table 2.11 Per-unit electrical parameter of smoothing capacitance

Smoothing Capacitance (pu)
18.76

Table 2.12 Per-unit electrical parameter of three-phase voltage source

Phase-to-phase Voltage KV	Source Resistance pu	Source Inductance pu
3.3	0.082	0.4783

2.3 Simulation of the System

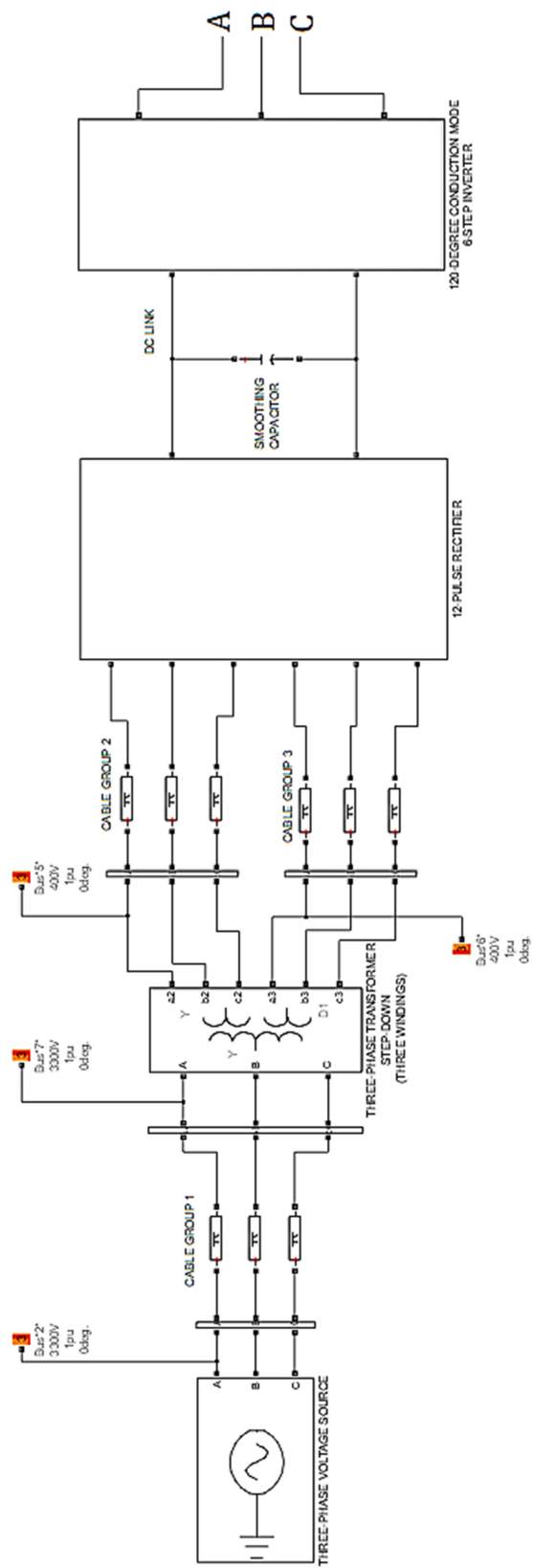


Figure 2.23 The analyzed 3-phase medium voltage power system

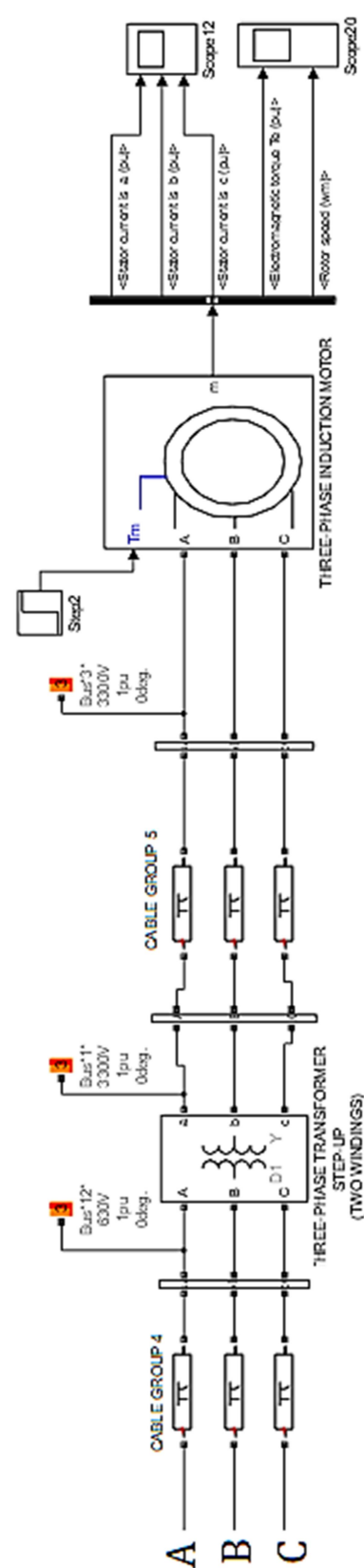


Figure 2.23 continues

The simulink model of the system is shown in Figure 2.23. The engine was idle for a while until it stabilized and a load of 1000 Nm was activated in the third second of the simulation. In this case, the output current and voltage waveforms of the rectifier are as in Figure 2.24.

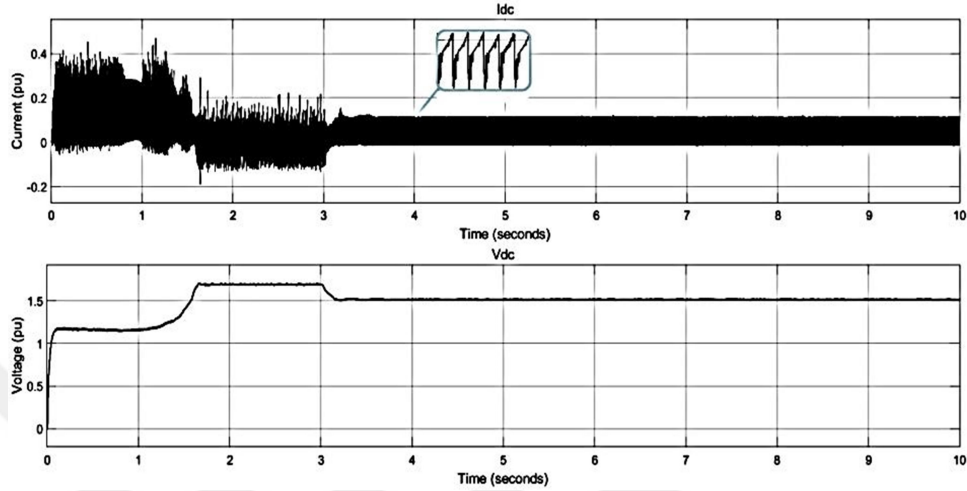


Figure 2.24 Output current and voltage waveforms of the 12-pulse rectifier

The inverter output line-to-line voltages are as shown in Figure 2.25. As seen, the output waveform is similar to the output of 180 degrees, although the inverter is commuted with 120 degrees, with the effect of the inductive transformer and motor connected to its output. Figure 2.26 shows the waveforms of the inverter output current. As can be seen, a discontinuous flow pattern is obtained.

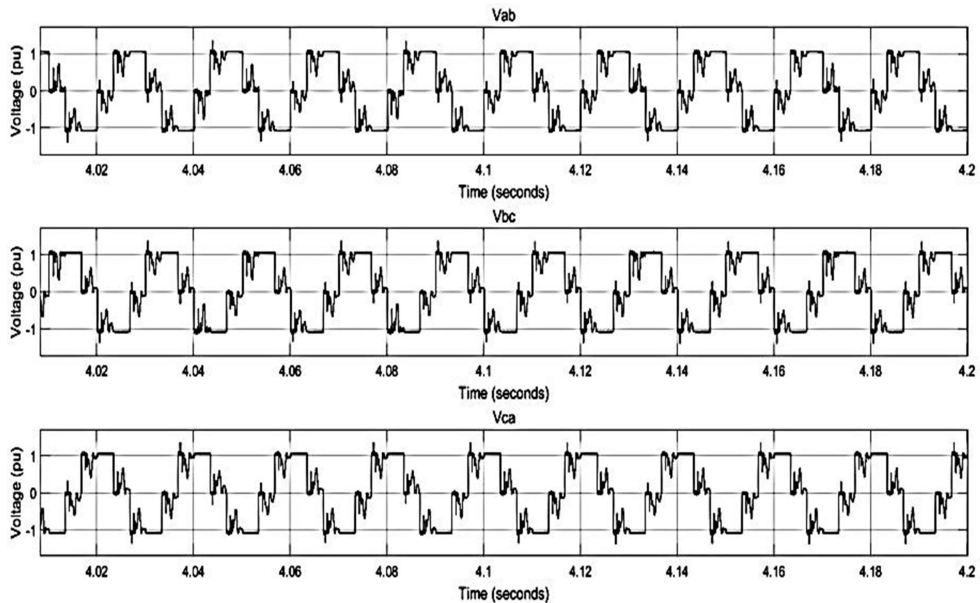


Figure 2.25 Output line-to-line voltage waveforms of the inverter

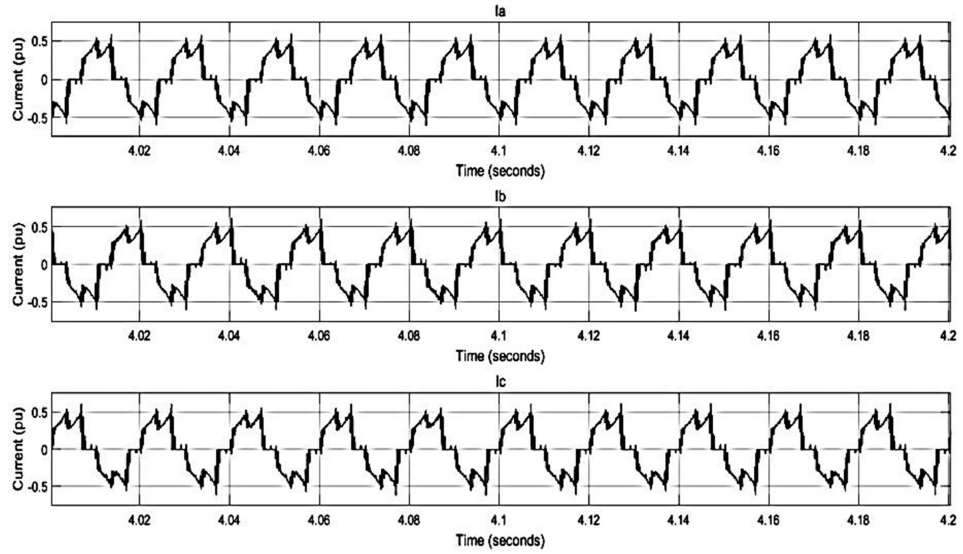


Figure 2.26 Output current waveforms of the inverter

Figure 2.27 shows the motor terminal voltage waveforms. As shown in the figure, the inverter output waveform is transformed into a different format using delta-wye connection of the step-up transformer. Motor stator current waveforms are as in Figure 2.28. These waveforms are obtained with no load. When the load is activated, the shape of the current around the value of 0 becomes slightly steep and the waveforms become as shown in Figure 2.29.

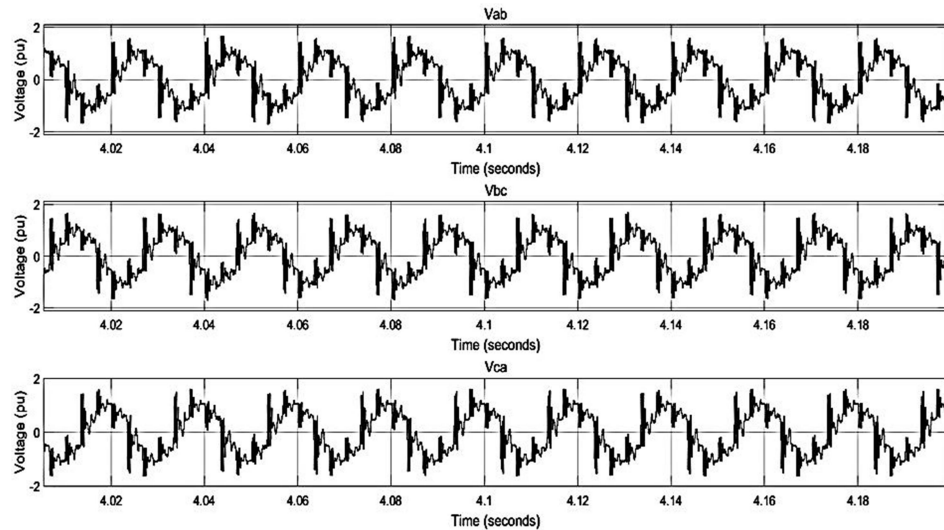


Figure 2.27 Voltage waveforms of the motor terminals

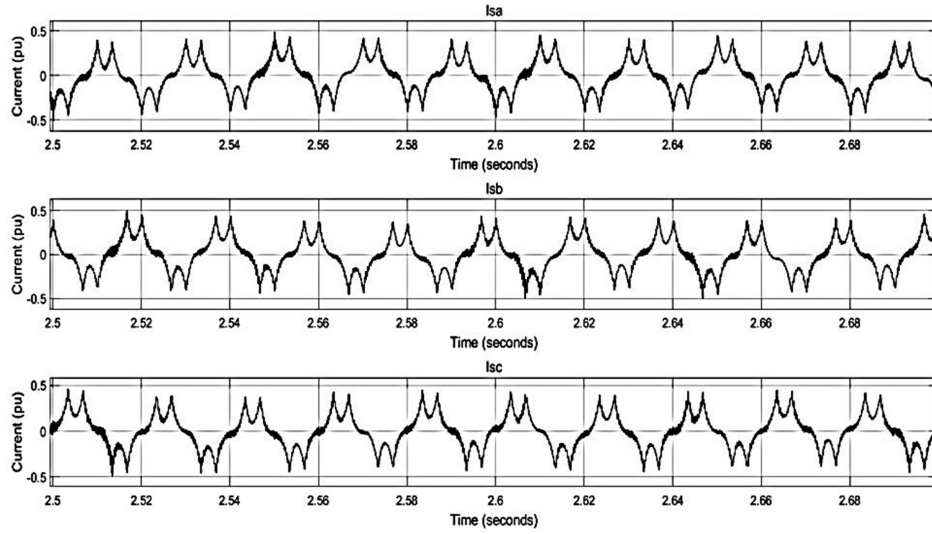


Figure 2.28 Stator current waveforms of the motor (with no load)

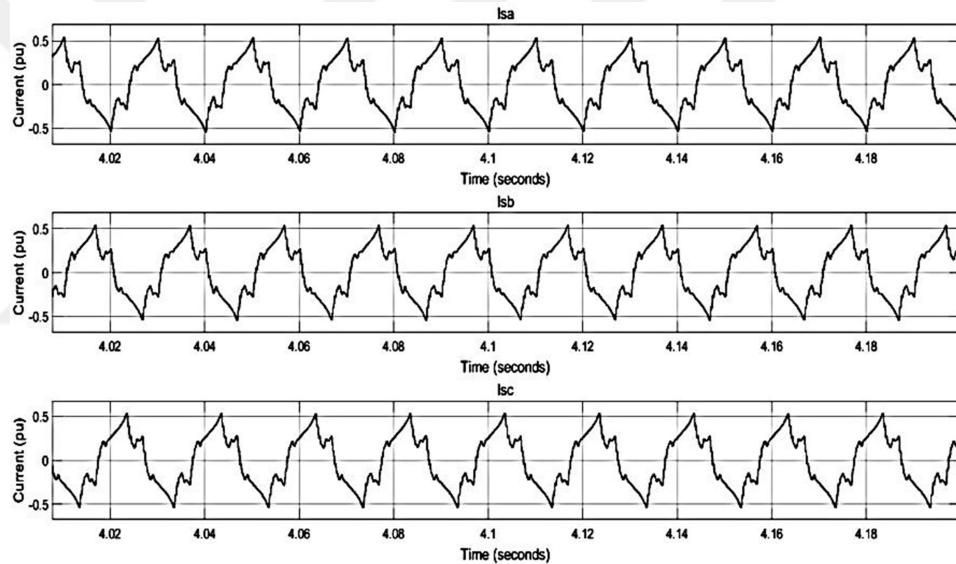


Figure 2.29 Stator current waveforms of the motor (with load)

The torque and speed of the driven motor will change as shown in Figure 2.30. The relationship between torque and speed (torque-speed characteristics) is as in Figure 2.31 for different frequencies.

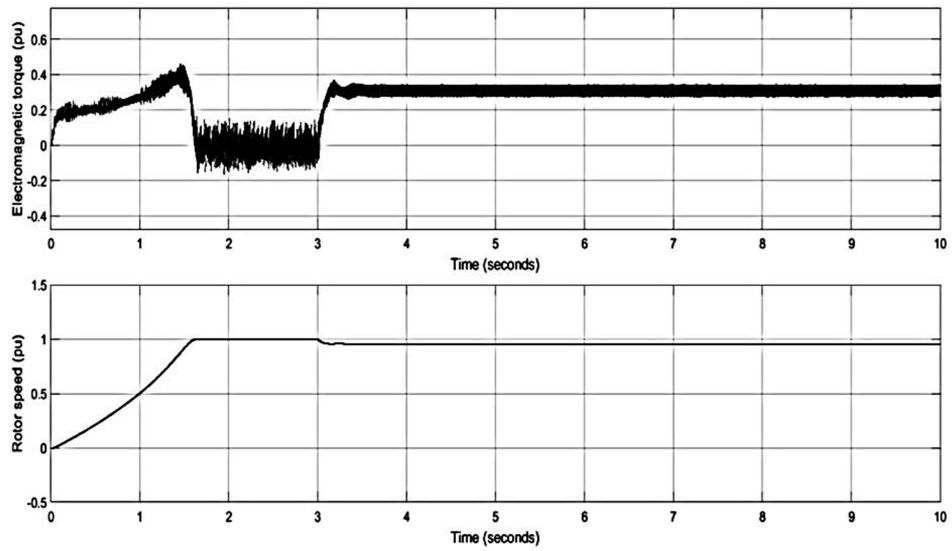


Figure 2.30 Torque and speed graphs of the motor

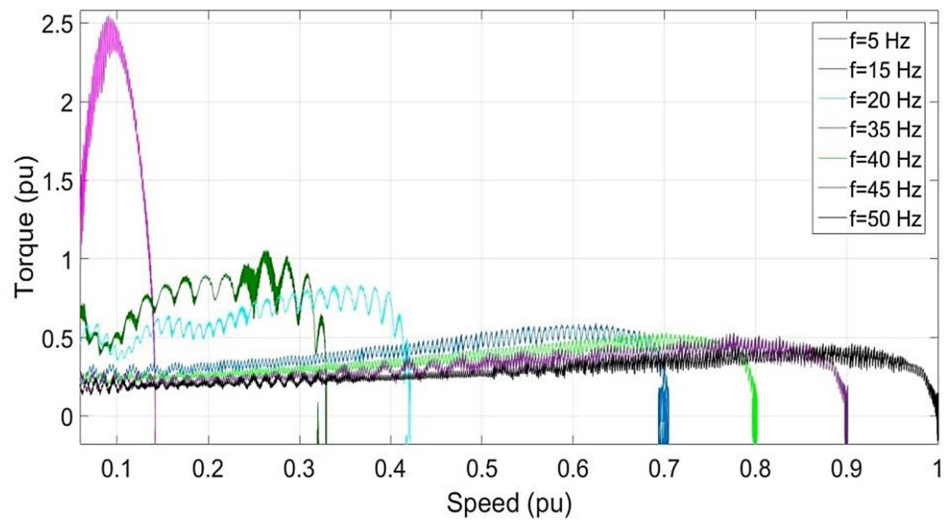


Figure 2.31 The relationship between torque and speed at different frequencies

CHAPTER THREE

RESONANCE ANALYSIS

The system comprises power electronic circuits, i.e. drive, which consists of nonlinear semiconductor elements, which control the motor speed, frequency, and torque, as described in chapter two. The motor draws non-sinusoidal current from the system depending on the switching period of the switches contained in the drive. The magnetic circuits of the motor and the loads entering and leaving the system are also effective in the formation of this non-sinusoidal current waveform. In addition, the magnetizing currents of the transformer play a role in the formation of this waveform. In this case, the current does not consist only of a single component at the fundamental frequency (50 Hz). The current contains components with frequencies that are multiples of the fundamental frequency. These components are called harmonics. Harmonic currents are the source of torque and speed fluctuations on the motor, and also the source of possible resonance in the system.

The reactance values of the capacitive elements in the system decrease with the effect of high-frequency harmonics. The currents that they draw at harmonic frequencies increase due to the reduction of reactance. The current amplitude is increased by harmonics and it may exceed the rated value of the capacitor and lead to puncture in the capacitor's insulation. In cables, they can reduce the real current capacity by the effect of the reactive component increased. Harmonics can cause overheating and power loss in inductive elements such as transformers and motors. In motors, they can also cause speed and torque oscillations and even noise. In the control and protection elements, they can cause malfunctions in electronic boards and unwanted tripping. As a result, they weaken the insulation of the elements and shorten their service life, making the system more insecure and inefficient. Resonance is the most important part of the problems worsen this situation that they can create.

In a system containing inductance and capacitance and which is supplied with a current or voltage containing harmonic components, the equalization of inductive and capacitive reactance values at a certain frequency is called resonance. At the time of resonance, as can be understood from its definition, the magnitude of the

total capacitive reactance of the system is equal to the magnitude of the total inductive reactance. However, since they are in opposite phases, they eliminate each other and the reactive component (imaginary component) of the impedance becomes zero. Resonance occurs when the system impedance consists only of real terms. Also, in this case, the phase difference (angle) between current and voltage is expected to be zero (Wang, 2010). Depending on the structure of the system, the resonance may be characteristic of two differences: series and parallel. In the case of series resonance, the impedance value is expected to decrease to a minimum and the current value is expected to increase to the maximum value. In the case of parallel resonance, the impedance is expected to reach its maximum value, as opposed to expected in the case of series resonance. From this point of view, it can be understood that the main factor determining the resonance conditions is impedance. Thus, resonance status can be determined by calculating the impedance of the system and examining the behavior according to the frequency. Analytical methods and simulation can be used for this purpose.

3.1 Determination of Resonance Frequency

3.1.1 Solution Method with the Reactive Component of the Impedance

As discussed in Chapter 2, the voltage controlled DC link has a decoupling capacitor. The capacitor that is between the rectifier and inverter supplies instantaneous current difference at the zero average level between the rectifier output and inverter input. Since there is no dominant element, such as a long cable, on the AC power supply side, the rectifier side may be considered to have no effect on a resonance condition that may occur at the motor terminals. Therefore, the resonance evaluation is made by considering the inverter, transformer and motor (load group) side. A parallel resonance causes overvoltages that may appear at the motor terminal or/and cable creating damage on the insulation. Thus, in order to determine the impedance of the system, the output of the drive is assumed to be an AC voltage source and the single phase equivalent circuit of the system is formed as in Figure 3.1. The parameters of the load model are given in Table 2.3, Table 2.1 and Table 2.4, respectively.

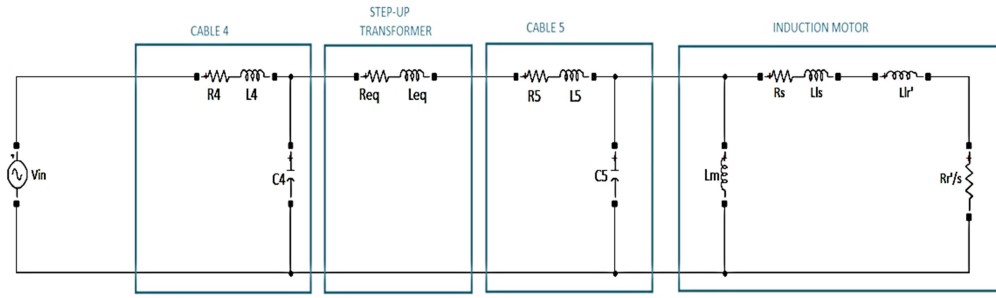


Figure 3.1 Load model of the system

Where

$$R_{eq} = R_1 + a^2 R_2$$

$$X_{eq} = X_1 + a^2 X_2$$

$$a^2 = \left(\frac{N_1}{N_2}\right)^2$$

In the model shown in Figure 2.24, the length of the cables in group 4 is very short compared to the cables in group 5. Therefore, there will be almost no significant impact on the resonance. This cable group can be neglected and the model can be simplified by collecting the same type of series components in the same arms, as in Figure 3.2.

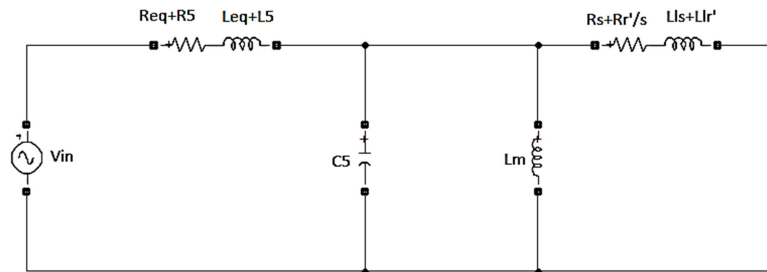


Figure 3.2 The simplified load model

In the circuit shown in Figure 3.2, when the norton transformation is made, the circuit takes the following form.

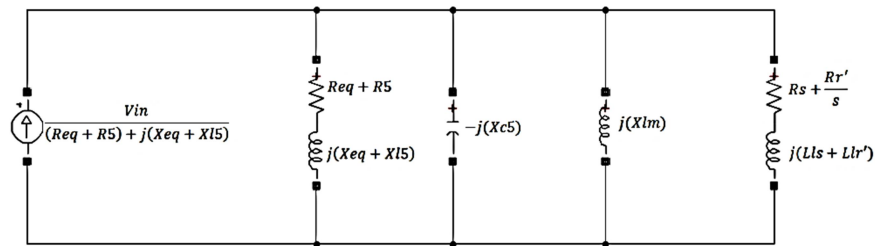


Figure 3.3 Norton equivalent circuit of the load model

The following expressions were used instead of components in the arms shown in Figure 3.3 and the final version of the equivalent circuit is as in Figure 3.4.

$$I = \frac{V_{in}}{(R_{eq} + R_5) + j(X_{eq} + X_{L_5})}$$

$$R_T = R_{eq} + R_5$$

$$X_{L_T} = X_{eq} + X_{L_5}$$

$$X_C = X_{C_5}$$

$$R_{TM} = R_s + \frac{Rr'}{s}$$

$$X_{L_{TM}} = X_{L_{ls}} + X_{L_{lr}}$$

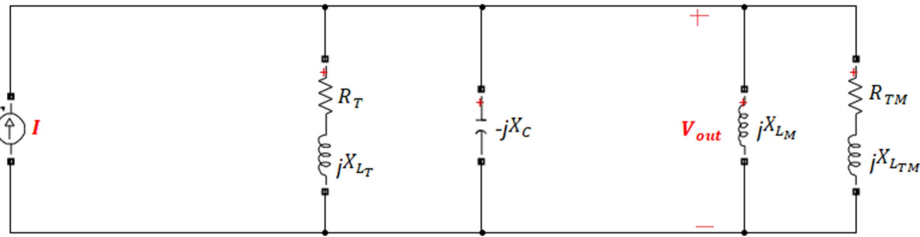


Figure 3.4 The analyzed load model

Figure 3.4 shows that the system resembles a parallel resonance circuit. The impedance of the system can be calculated as follows according to Figure 3.4.

$$\frac{1}{Z} = \frac{1}{R_T + jX_{L_T}} + \frac{1}{-jX_C} + \frac{1}{jX_{L_M}} + \frac{1}{R_{TM} + jX_{L_{TM}}} \quad (3.1)$$

$$= \frac{R_T - jX_{L_T}}{R_T^2 + X_{L_T}^2} + \frac{jX_C}{X_C^2} - \frac{jX_{L_M}}{X_{L_M}^2} + \frac{R_{TM} - jX_{L_{TM}}}{R_{TM}^2 + X_{L_{TM}}^2} \quad (3.2)$$

$$= \left(\frac{R_T}{R_T^2 + X_{L_T}^2} + \frac{R_{TM}}{R_{TM}^2 + X_{L_{TM}}^2} \right) + j \left(\frac{-X_{L_T}}{R_T^2 + X_{L_T}^2} + \frac{X_C}{X_C^2} - \frac{X_{L_M}}{X_{L_M}^2} - \frac{X_{L_{TM}}}{R_{TM}^2 + X_{L_{TM}}^2} \right) \quad (3.3)$$

The imaginary component of the admittance value is 0, it provides information about the resonance (Wang, 2010). According to this;

$$\text{If } \text{Im}\left(\frac{1}{Z}\right) = \text{Im}(Y) = 0;$$

$$\frac{-X_{L_T}}{R_T^2 + X_{L_T}^2} + \frac{1}{X_C} - \frac{1}{X_{L_M}} - \frac{X_{L_{TM}}}{R_{TM}^2 + X_{L_{TM}}^2} = 0 \quad (3.4)$$

Hence,

$$\frac{-X_{L_T} \cdot X_C \cdot X_{L_M} (R_{TM}^2 + X_{L_{TM}}^2) + (R_T^2 + X_{L_T}^2) \cdot X_{L_M} (R_{TM}^2 + X_{L_{TM}}^2) - (R_T^2 + X_{L_T}^2) \cdot X_C (R_{TM}^2 + X_{L_{TM}}^2) - X_{L_{TM}} (R_T^2 + X_{L_T}^2) \cdot X_C \cdot X_{L_M}}{(R_T^2 + X_{L_T}^2) \cdot X_C \cdot X_{L_M} (R_{TM}^2 + X_{L_{TM}}^2)} = 0 \quad (3.5)$$

Therefore,

$$\begin{aligned}
& -X_{L_T} \cdot X_C \cdot X_{L_M} \cdot R_{TM}^2 - X_{L_T} \cdot X_C \cdot X_{L_M} \cdot X_{L_{TM}}^2 + R_T^2 \cdot X_{L_M} \cdot R_{TM}^2 + R_T^2 \cdot X_{L_M} \cdot X_{L_{TM}}^2 + X_{L_T}^2 \cdot X_{L_M} \cdot R_{TM}^2 + X_{L_T}^2 \cdot X_{L_M} \cdot X_{L_{TM}}^2 \\
& - R_T^2 \cdot X_C \cdot R_{TM}^2 - R_T^2 \cdot X_C \cdot X_{L_{TM}}^2 - X_{L_T}^2 \cdot X_C \cdot R_{TM}^2 - X_{L_T}^2 \cdot X_C \cdot X_{L_{TM}}^2 - X_{L_{TM}} \cdot X_C \cdot X_{L_M} R_T^2 - X_{L_{TM}} \cdot X_C \cdot X_{L_M} X_{L_T}^2 = 0 \quad (3.6)
\end{aligned}$$

where

$$\begin{aligned}
X_{L_T} &= \omega \cdot L_T \\
X_C &= \frac{1}{\omega \cdot C} \\
X_{L_M} &= \omega \cdot L_M \\
X_{L_{TM}} &= \omega \cdot L_{TM}
\end{aligned}$$

$$\begin{aligned}
& -\omega \cdot L_T \cdot \frac{1}{\omega C} \cdot \omega \cdot L_M \cdot R_{TM}^2 - \omega \cdot L_T \cdot \frac{1}{\omega C} \cdot \omega \cdot L_M \cdot (\omega \cdot L_{TM})^2 + R_T^2 \cdot \omega \cdot L_M \cdot R_{TM}^2 + R_T^2 \cdot \omega \cdot L_M \cdot (\omega \cdot L_{TM})^2 + (\omega \cdot L_T)^2 \cdot \omega \cdot L_M \cdot R_{TM}^2 + \\
& (\omega \cdot L_T)^2 \cdot \omega \cdot L_M \cdot (\omega \cdot L_{TM})^2 - R_T^2 \cdot \frac{1}{\omega C} \cdot R_{TM}^2 - R_T^2 \cdot \frac{1}{\omega C} \cdot (\omega \cdot L_{TM})^2 - (\omega \cdot L_T)^2 \cdot \frac{1}{\omega C} \cdot R_{TM}^2 - (\omega \cdot L_T)^2 \cdot \frac{1}{\omega C} \cdot (\omega \cdot L_{TM})^2 - \\
& (\omega \cdot L_{TM})^2 \cdot \frac{1}{\omega C} \cdot \omega \cdot L_M \cdot R_T^2 - \omega \cdot L_{TM} \cdot \frac{1}{\omega C} \cdot \omega \cdot L_M (\omega \cdot L_T)^2 = 0 \quad (3.7)
\end{aligned}$$

Hence,

$$\begin{aligned}
& \omega^6 (L_T^2 L_M L_{TM}^2) + \omega^4 \left(-\frac{L_T L_M L_{TM}}{C} + R_T^2 L_M L_{TM}^2 + L_T^2 L_M R_{TM}^2 - L_T^2 L_{TM}^2 - L_{TM}^2 L_M L_T^2 \right) + \\
& \omega^2 \left(-\frac{L_T L_M R_{TM}^2}{C} + R_T^2 L_M R_{TM}^2 - R_T^2 L_{TM} - L_T^2 R_{TM}^2 - L_{TM} L_M R_T^2 \right) + (R_T^2 R_{TM}^2) = 0 \quad (3.8)
\end{aligned}$$

The roots of this equation are calculated with the commands given in Appendix 2.

The solution of the sixth order equation gives the following roots.

$$\omega = 10^4 \times \begin{bmatrix} -1.8212 + j0.0000 \\ 1.8212 + j0.0000 \\ 0.0000 + j0.1755 \\ 0.0000 - j0.1755 \\ -0.0000 + j0.0000 \\ -0.0000 - j0.0000 \end{bmatrix} rad/s$$

For any of the calculated root values to be considered as ω_0 that resonance occurs, the value must be greater than zero and real (Wang, 2010). Accordingly, the appropriate root and the frequency value at which the resonance can occur is as follows.

$$\omega_0 = 18212 \text{ rad/s}$$

$$f_0 = \frac{\omega_0}{2\pi} = 2898 \text{ Hz}$$

3.1.2 Bode Diagram

Bode diagram is a method that gives information about how the amplitude and phase of the inputs related to the system will change depending on the frequency. The frequency response of this system between the motor input and the inverter output can be expressed as in equation (3.9) using Figure 3.4. As can be seen, the transfer function examined corresponds to the impedance of the system. Information about resonance can be obtained by examining the change of impedance with frequency.

$$Z(j\omega) = \frac{V_{out}}{I_{in}}(j\omega) \quad (3.9)$$

In the Bode diagram shown in Figure 3.5. Variation of both the magnitude of the impedance and the phase angle with frequency can be seen in this diagram. When the phase angle is 0, it is seen that the impedance value reaches the maximum. This is the expected case during parallel resonance. The peak value of the impedance corresponds to the parallel resonance frequency. Accordingly, the predicted resonance frequency is as follows.

$$f_{peak} = 2850 \text{ Hz}$$

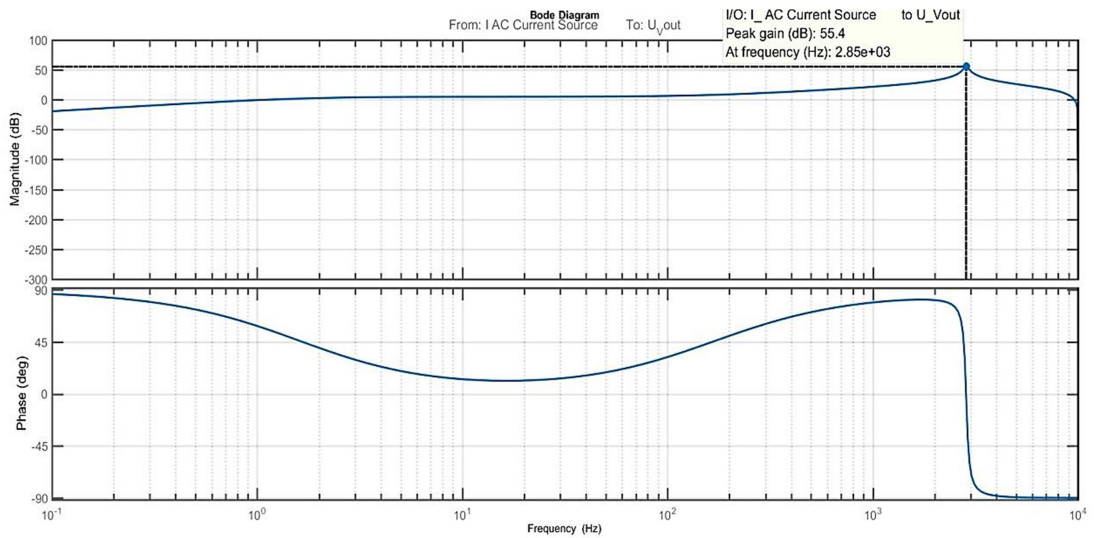


Figure 3.5 Bode diagram

3.1.3 General Resonance Frequency Formula

The total capacitive reactance at the time of resonance and the total inductive reactance will be equal in the case of a parallel resonance, hence the resonance frequency can be calculated as follows.

$$\frac{1}{Z} = \frac{1}{j\omega L_{total}} + \frac{1}{-j\left(\frac{1}{\omega C_{total}}\right)} \quad (3.10)$$

$$= -j\left(\frac{1}{\omega L_{total}}\right) + j(\omega C_{total}) \quad (3.11)$$

If $X_{Ltotal} = X_{Ctotal}$;

$$\frac{1}{\omega_0 L_{total}} = \omega_0 C_{total} \quad (3.12)$$

Hence,

$$\omega_0 = \frac{1}{\sqrt{(L_{total} C_{total})}} \quad (3.13)$$

and so,

$$f_r = \frac{1}{2\pi\sqrt{(L_{total} C_{total})}} \quad (3.14)$$

Equation 3.14 is a general formula used to calculate the resonance frequency. However, the resistive components in the system are generally ignored in this equation.

According to formula (3.14) and according to parameters in Table 2.3, Table 2.1 and Table 2.4, the resonance frequency can be calculated as follows;

Where

$$\begin{aligned} L_{total} &= L_T // L_M // L_{TM} \\ &= \frac{1}{\frac{1}{L_T} + \frac{1}{L_M} + \frac{1}{L_{TM}}} \\ &= \frac{1}{\frac{1}{L_1 + a^2 L_2 + L_5} + \frac{1}{L_M} + \frac{1}{L_{ls} + L_{lr'}}} \end{aligned}$$

$$\begin{aligned}
&= \frac{1}{\left(\frac{1}{7.5802 \times 10^{-5} + \left(\frac{630}{3300} \right)^2 \times 6.9328 \times 10^{-4} + 5 \times 0.351 \times 10^{-3}} \right) + \frac{1}{0.1749} + \frac{1}{(7.7445 \times 10^{-3} + 9.5111 \times 10^{-3})}} \\
&= \frac{1}{\frac{1}{1.9066 \times 10^{-3}} + \frac{1}{0.1749} + \frac{1}{0.0173}} \\
&= \frac{1}{524.4939 + 5.7176 + 57.8035} \\
&= 1.7 \times 10^{-3} \text{ H}
\end{aligned}$$

where

$$\begin{aligned}
C_{total} &= C_5 \\
&= 5.0318. 10^{-6} \\
&= 1.59. 10^{-6} \text{ F}
\end{aligned}$$

The resonance frequency is obtained as follows;

$$\begin{aligned}
f_r &= \frac{1}{2\pi\sqrt{(1.7 \times 10^{-3} \times 1.59 \times 10^{-6})}} \\
&= 3061 \text{ Hz}
\end{aligned}$$

According to the generalized formula, the expected resonance frequency is 3061 Hz. It is seen that it is about 200 Hz different from the results calculated according to bode diagram and the formula obtained from the equivalent circuit of the system. This formula is obtained by ignoring the effect of all components except inductive and capacitive components in the system. However, there are factors such as the damping effect of resistive components. Therefore, the other methods can be considered to be more accurate.

3.1.4 FFT Analysis

The predicted resonance frequency value according to the single phase equivalent circuit of the system is approximately 2850 Hz. (2898 Hz was found in the analytical solution, 2850 Hz was found in the Bode diagram). In order to determine whether this evaluation corresponds to the actual system, the motor terminal voltages can be examined in the simulation of the main power system shown in Figure 2.23. When the FFT analysis of the terminal voltages is performed, it is seen that the frequency

of the harmonic components of the voltage is concentrated around the resonance frequency of the system and the amplitudes are increased as shown in Figure 3.6. The resonance frequency corresponds to approximately 57th harmonic.

$$\% hf = \left| \frac{\frac{1}{57}}{1} \right| \cdot 100 = 1.75 \%$$

The percentage value of this harmonic can be normally around 1.75%, as can be seen above calculation, according to the simplified equation (2.6) but it increases up to 15% in the analyzed system.

The parallel resonance state is characterized by the bandwidth, the interval between critical frequency values, and quality factor, expressed in equation (3.15) and equation (3.16), respectively (Wang, 2010).

$$BW = f_2 - f_1 = \frac{f_r}{Q} \quad (3.15)$$

$$Q = \frac{R}{X_C} = \frac{R}{X_L} \quad (3.16)$$

According to Appendix 3, the total resistance (R) value is 1.8128 Ω and the total inductance (L) value is 0.0017 H approximately. Accordingly, the quality factor and bandwidth are as follows.

$$Q = \frac{1.8128}{(2 \times \pi \times 50 \times 0.0017)} = 3.6036$$

$$BW = \frac{2850}{3.6036} = 790.8758$$

Both critical frequency values are at an equal distance to the resonant frequency. Hence;

$$f_1 = f_r - \frac{BW}{2} = 2850 - \frac{790.8758}{2} = 2454.6 \text{ Hz}$$

$$f_2 = f_r + \frac{BW}{2} = 2850 + \frac{790.8758}{2} = 3245.4 \text{ Hz}$$

In Figure 3.6, it can be seen that there is a rising approximately between critical resonance values.

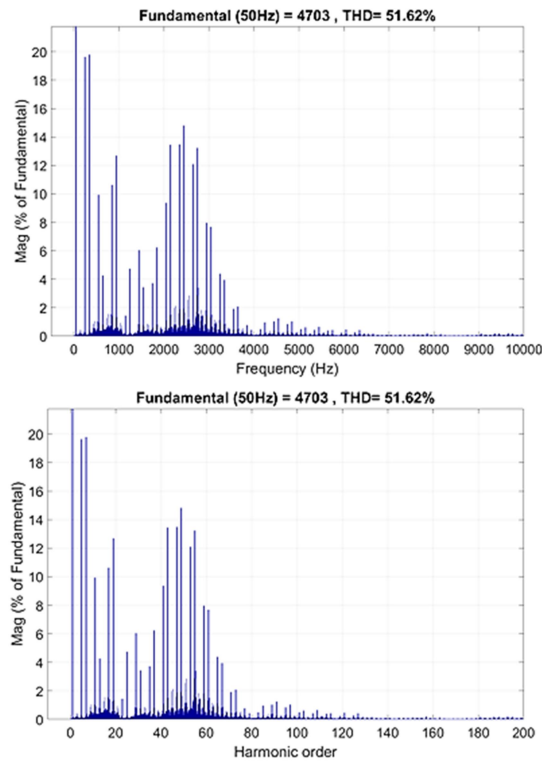


Figure 3.6 FFT analysis of motor terminal voltage

In addition, this resonance occurring at the motor terminal will be reflected in the inverter current. This can be seen from the FFT analysis shown in Figure 3.7.

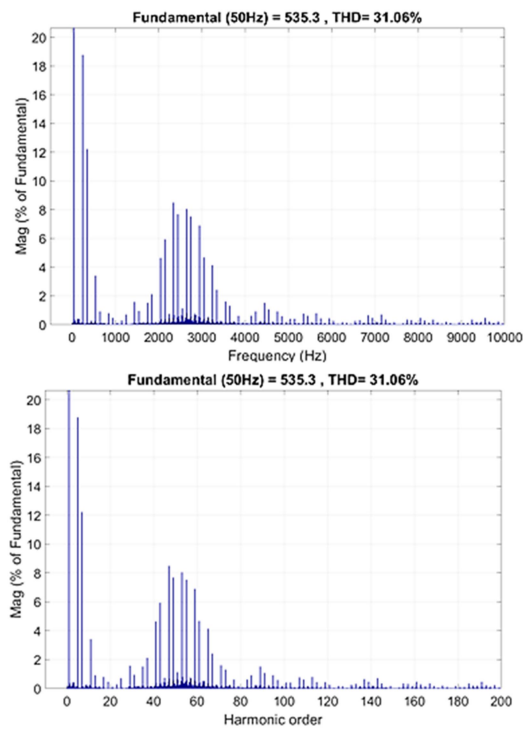


Figure 3.7 FFT analysis of inverter output current

3.2 Factors Affecting Resonance Conditions

3.2.1 Effects of Cable Length on Resonance

The length of the power cables feeding the motor is changed to 1, 2, 3, 4, 5, 6, 7, 8, 9 and 10 km respectively. In this case, according to the Bode diagram analysis of the simplified single-line equivalent circuit, the frequency response of the system changes as in Figure 3.8. At the same time, the cable lengths have been changed in three-phase power system simulation. In this case, the FFT analysis of the harmonics occurring at the motor terminal voltage is as in Figure 3.9.

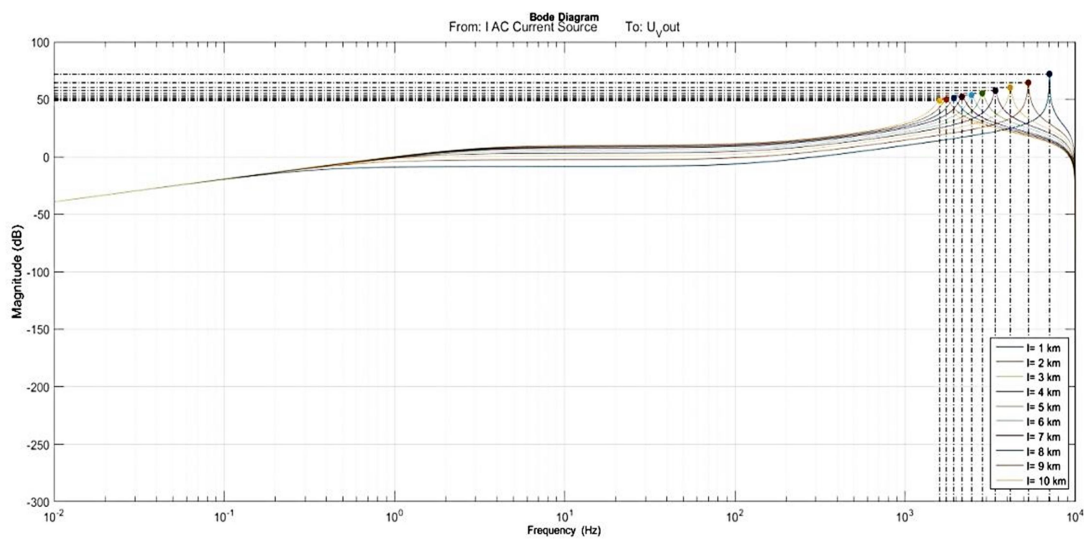


Figure 3.8 Bode diagram results according to various cable lengths

As shown in Figure 3.8, as the cable length is increased, the peak of the Bode diagram shifts to the left. In Figure 3.9, when the cable length is 1 km, it can be seen that the harmonics whose percentage sizes decrease while the frequency increases, show a rise again around 5300 Hz. When the cable is 2 km, this point where the harmonics are concentrated has shifted to around 4200 Hz. When a 3 km cable is used, the harmonics are concentrated around 3500 Hz. When the cable length is 4 km, it is observed that this point, where the harmonics rise, goes even further and takes place around 3000 Hz. When the cable length is 5 km, the point at which this harmonic density occurs falls below 3000 Hz. When the cable size is increased further, it is observed that this shifting tendency observed in FFT analysis continues and when the cable length is selected as 10 km, this concentration point, which was initially observed at values above 5000 Hz, falls below 2000 Hz.

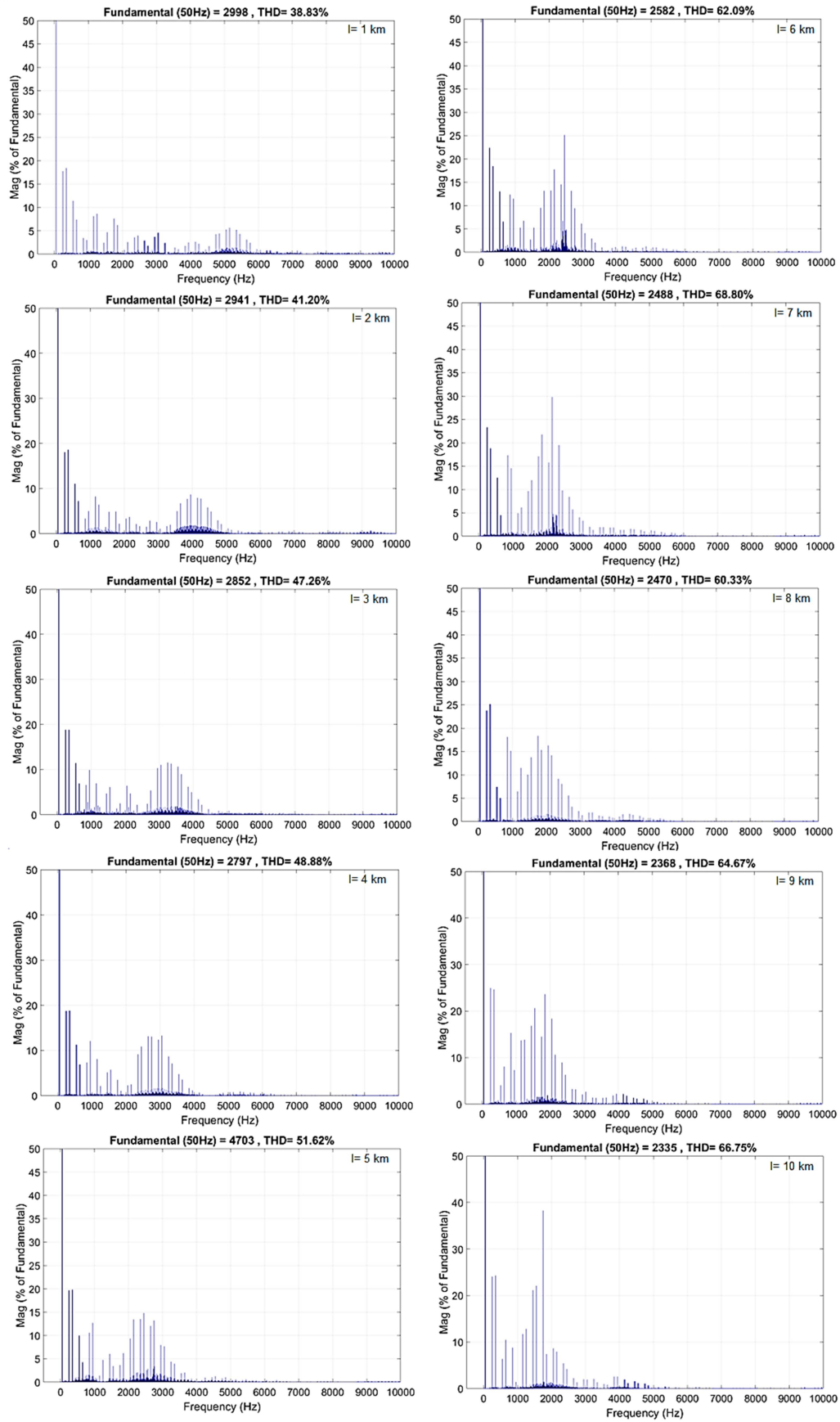


Figure 3.9 FFT results according to various cable lengths

The results obtained from Bode diagram and FFT analysis, and the results to be obtained in different cable lengths according to analytical solutions are summarized in Figure 3.10.

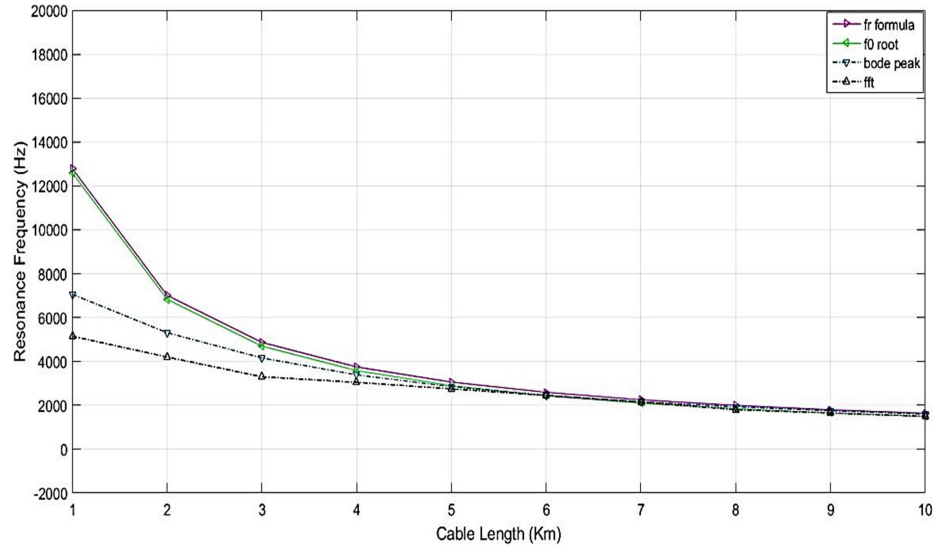


Figure 3.10 Change of resonance frequency according to cable length

It can be seen in Figure 3.10 that the expected tendency of change in resonance frequency is in the same direction according to all methods. Consequently, it can be said that as the size of the cable used increases, the frequency at which resonance can occur decreases.

The increase in cable length increases active power losses due to the increase in cable resistance. But more importantly, as the cable length increases, it is known that the cable component whose value becomes the most dominant is capacitance. Even that in some major power systems, long cables can be modeled as only capacitances, while other components are omitted. Therefore, it can be said that the main factor that causes the expected resonance frequency to change is the change in cable capacitance.

At low frequencies, percent magnitudes values of the lower order harmonic of the system are higher, as can be understood in equation (2.6). Therefore, if the harmonics of the system coincide with the resonance frequency, these harmonics can be more dangerous and destructive than the higher order harmonics. Hence, as the length of

the cable increases, the expected risk of the system will be greater in these cable sizes as the expected resonant frequency approaches the low order harmonics.

It can also be understood from these graphs that since a simplification is made based on the length of the selected cable (5 km) in the beginning, the most accurate results can be obtained after 5 km with these methods. Therefore, this should be taken into account when evaluating the resonance frequency, especially for short cables. However, the method that provides the most helpful result, in general, is the Bode diagram.

3.2.2 Effects of Motor Slip on Resonance

The slip on which the machine operates is one of the most important factors determining the operating mode of the machine. It is also closely related to the speed and torque of the machine as can be understood in equation (2.13). Although it is expected that motor-related parameters will not have a significant effect on resonance, it is important to know the effect of this parameter, even if it is small.

By selecting different slip values, frequency response of single line equivalent circuit of load model was investigated. When the motor is running at different slip values, the bode diagram is obtained as in Figure 3.11.

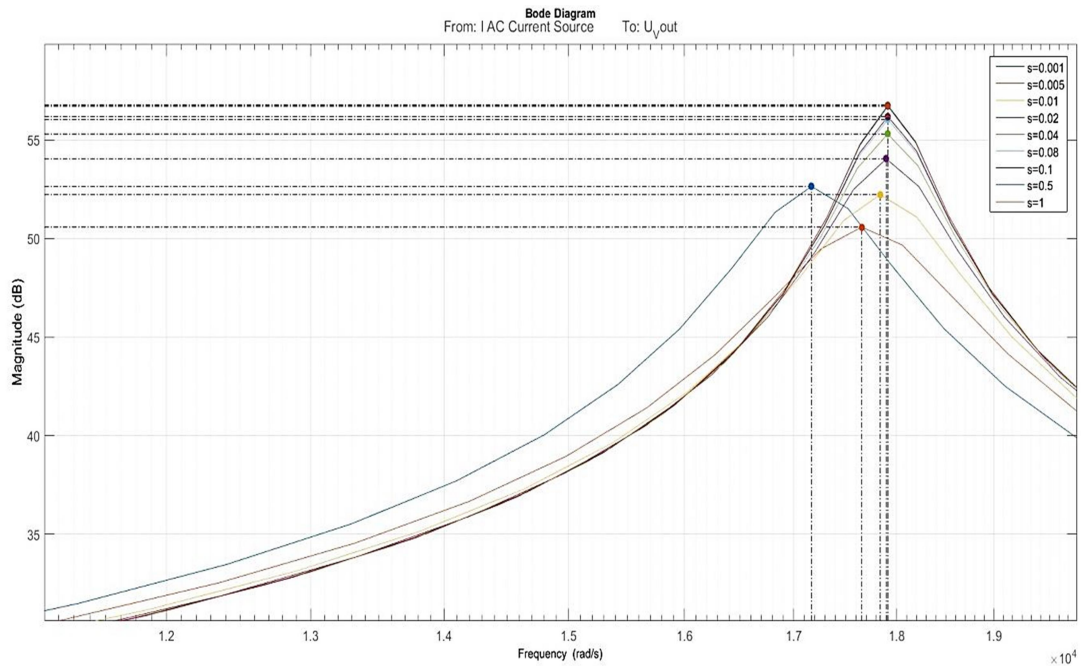


Figure 3.11 Bode diagram results at different slip values

The critical slip value of the motor according to equation (2.16) is as follows.

$$s_{max} = \frac{1.238}{[0.973^2 + (2.433 + 2.988)^2]^{\frac{1}{2}}}$$

$$s = 0.225$$

According to the analytical solution, the predicted resonance values in and around the critical resonance frequency are as in Table 3.1. According to these results, the results of the analytical solution and the bode diagram in the critical resonance and its surroundings are approximately matching. At the critical slip value and subsequent slip values, the roots obtained from equation 3.8 and the predicted resonance frequency are almost unchanged.

Table 3.1 Slip and root values

Slip	Roots	Expected resonance frequency
0.225	$-1.8131 \times 10^4 + j0.0000$	$f_0 \cong 2885 \text{ Hz}$
	$1.8131 \times 10^4 + j0.0000$	
	$0.0000 + j0.0375 \times 10^4$	
	$0.0000 - j0.0375 \times 10^4$	
	$-0.0000 + j0.0000$	
	$-0.0000 - j0.0000$	
0.5	$-1.8128 \times 10^4 + j0.0000$	$f_0 \cong 2885 \text{ Hz}$
	$1.8128 \times 10^4 + j0.0000$	
	$0.0000 + j0.0200 \times 10^4$	
	$0.0000 - j0.0200 \times 10^4$	
	$0.0000 + j0.0000$	
	$0.0000 - j0.0000$	
1	$-1.8127 \times 10^4 + j0.0000$	$f_0 \cong 2885 \text{ Hz}$
	$1.8127 \times 10^4 + j0.0000$	
	$-0.0000 + j0.0128 \times 10^4$	
	$-0.0000 - j0.0128 \times 10^4$	
	$0.0000 + j0.0000$	
	$0.0000 - j0.0000$	

According to these two approaches, especially the Bode Diagram, the variation of the resonance frequency with respect to the slip will be as in Figure 3.12. Accordingly, up to a certain slip value, the higher the slip value, the higher the expected resonance frequency. However, in fact, regardless of the size of the load, according to the slip, two basic different situations, no-load and with load, are experienced. Because only when s is very close to 0 (around 0.001) different values

were obtained, other than these, the results obtained were the same. Therefore, the expected resonance frequency will be different if the motor is idle ($f_r = 2730$ when $s = 0$). Otherwise, if the motor has reached rated speed and the load is activated, the expected resonance frequency will be the same as expected at the critical slip value even if the slip value is not known exactly. At this value, the expected resonance frequency from both methods will be approximately the same ($f_r = 2850$ when $s > 0$).

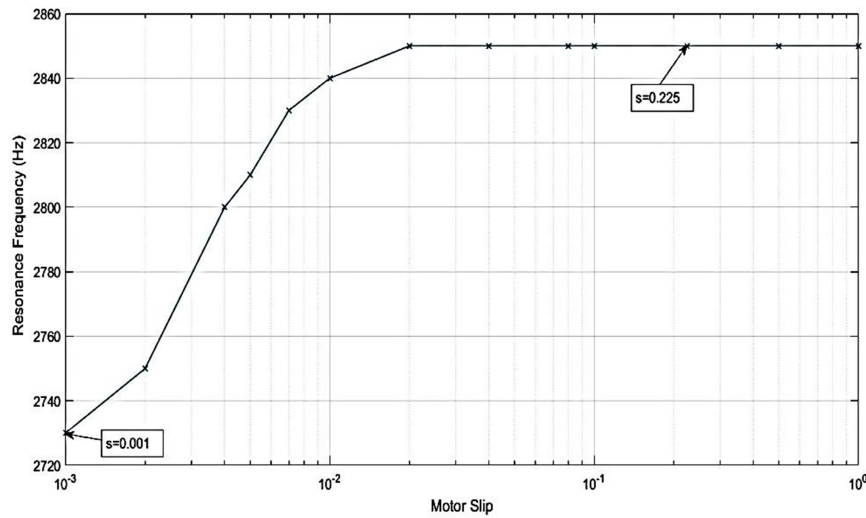
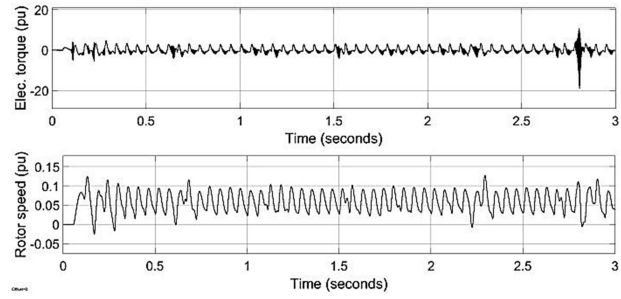


Figure 3.12 Slip and resonance frequency change

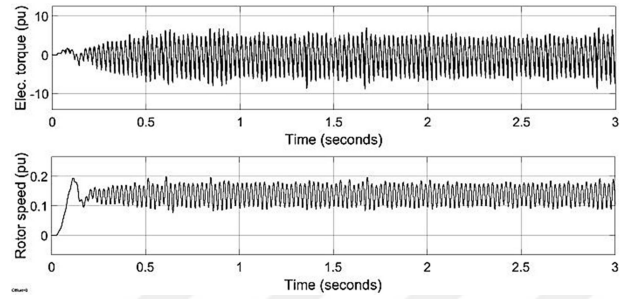
3.3 Resonance Conditions during Acceleration of the Motor

The motor cannot be started at the rated speed at one time. The motor driver of such systems has voltage/hertz control as specified in Chapter 2. So the frequency and speed of the motor are increased while maintaining the V/f ratio from the start until the motor reaches its nominal speed. Also, initially the electromagnetic torque is expected to be greater than the load torque for the motor to start. Otherwise, the motor will fall over.

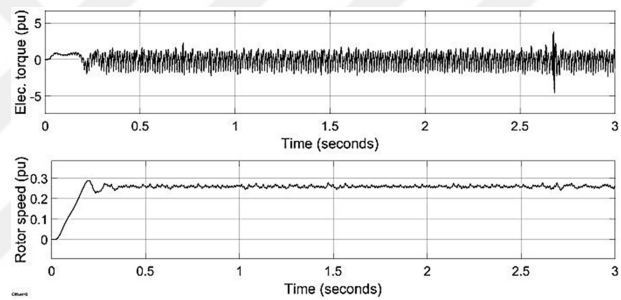
To understand the conditions that occurred during the start and whether a problem is encountered, the motor was operated for a while at various frequency levels before the load was switched on, in the simulation. While the motor is running at 3 Hz, 7 Hz, 13 Hz, 16 Hz, 22 Hz, 25 Hz, 30 Hz, 34 Hz, 41 Hz and 48 Hz respectively, torque and speed graphs are obtained as shown in Figure 3.13 and Figure 3.14.



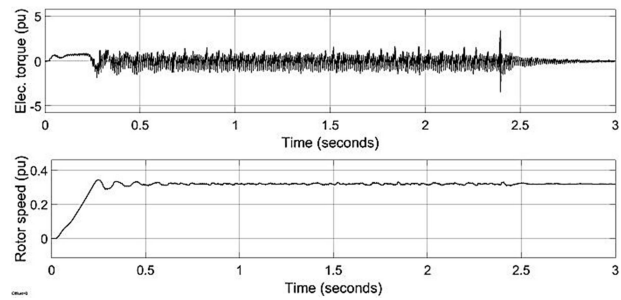
a)



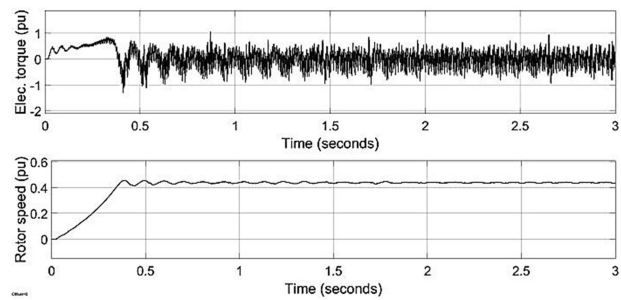
b)



c)



d)



e)

Figure 3.13 Torque and speed graphs at various frequencies a) 3 Hz b) 7 Hz c) 13 Hz d) 16 Hz e) 22 Hz

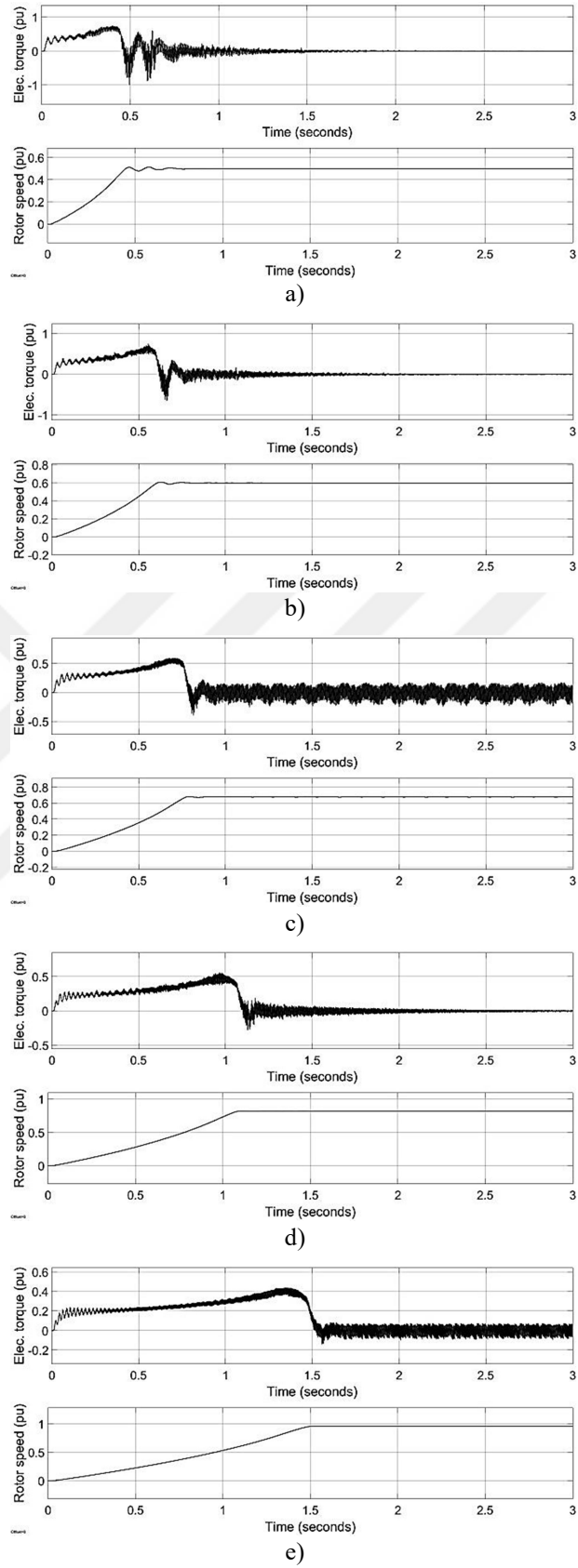


Figure 3.14 Torque and speed graphs at various frequencies a) 25 Hz b) 30 Hz c) 34 Hz d) 41 Hz e) 48 Hz

While the motor is driven at 3 Hz, the unusual torque fluctuation has happened after 2.5 seconds can be seen in Figure 3.13. A similar situation is also observed when the motor is running at 13 Hz. At 16 Hz, after a similar torque fluctuation, it is seen that the system could not recover and it has stopped producing torque. At 7 Hz and 22 Hz, despite the ripples of the torque and the speed, the system continues to operate without an extra high spike. In Figure 3.14, after the motor accelerated and reached 25 Hz, can not come to equilibrium and can not continue to produce torque is seen. A similar situation is experienced at 30 Hz and 41 Hz. In these frequencies, the torque values remain at 0 pu after a point and do not change. Conversely, while the motor is running at 34 Hz and 48 Hz, it stabilizes after acceleration and continues to produce torque.

The slip value is at the value of one at the starting. However, the slip value cannot reach 0 practically when the machine is running as a motor. For example, when the motor is idle at 50 Hz, it is observed that the motor speed varies between 1 and 0.999 pu. Therefore, the slip value is assumed to be 0.001. According to Figure 3.12, the resonance frequency of the system is about 2730 Hz while the slip is 0.001. In order to understand the cause of the different behaviors of the motor at different frequencies that are seen in torque and speed graphs, the motor terminal voltages were examined while the inverter was operating at 16, 25, 34 and 41 Hz. The distribution of the harmonics of the system at these frequencies is as in the figures 3.15, 3.16, 3.17 and 3.18 respectively.

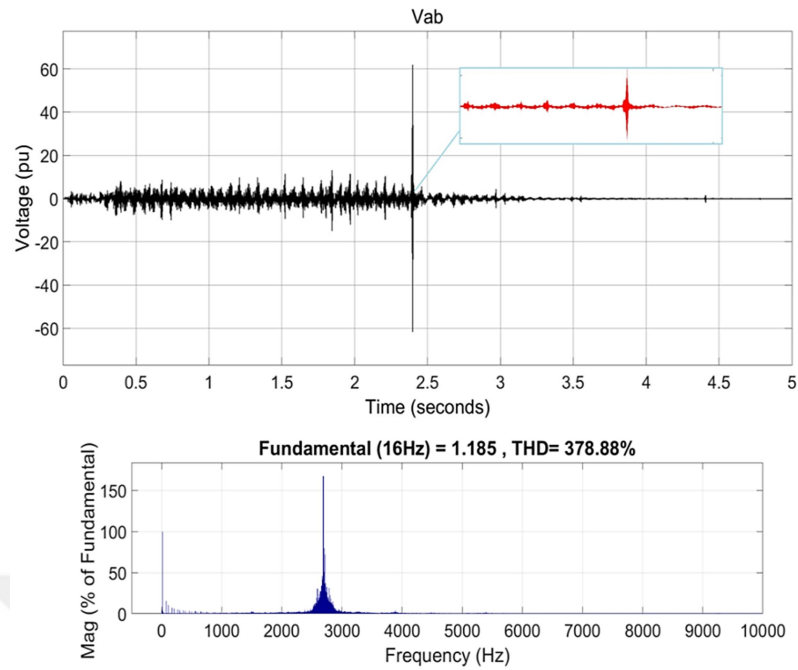


Figure 3.15 Motor terminal voltage and FFT analysis at 16 Hz

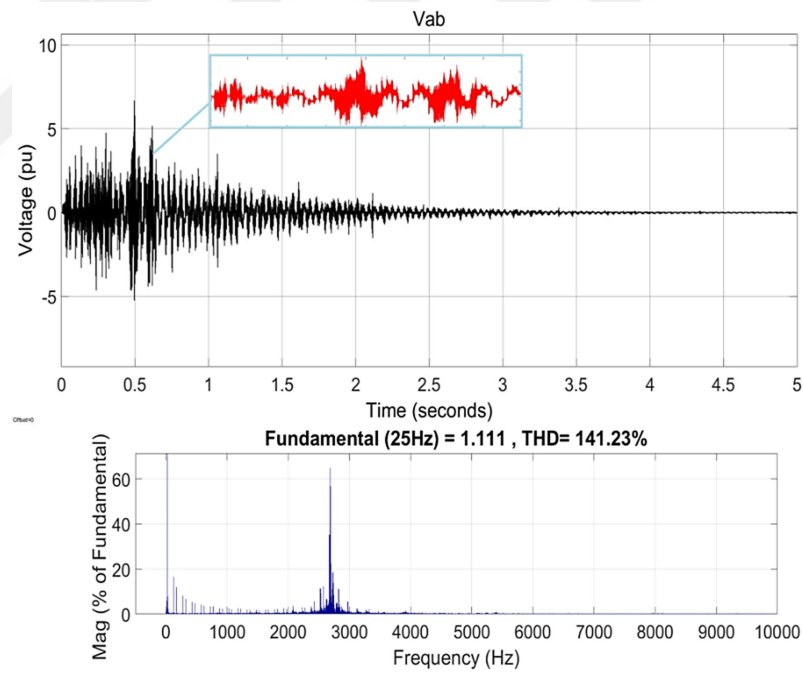


Figure 3.16 Motor terminal voltage and FFT analysis at 25 Hz

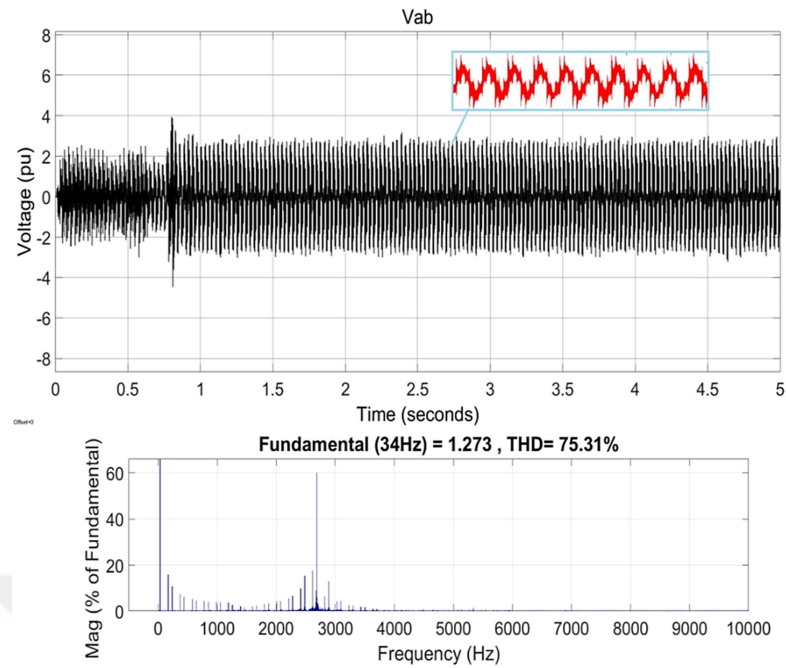


Figure 3.17 Motor terminal voltage and FFT analysis at 34 Hz

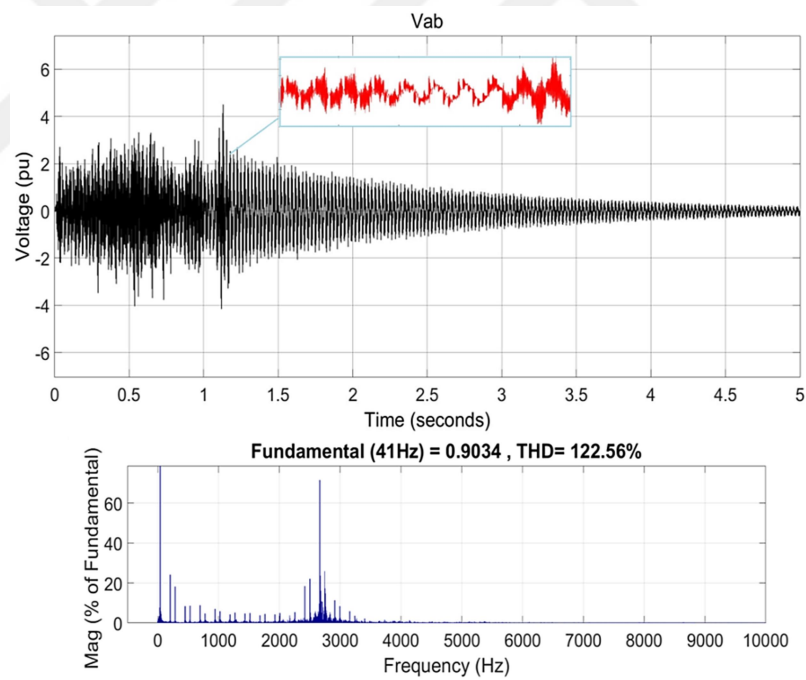


Figure 3.18 Motor terminal voltage and FFT analysis at 41 Hz

Figure 3.17 shows that the system continues to operate despite overvoltages when the operating frequency is 34 Hz. On the other hand, when the operating frequency is 16 Hz, the motor terminal voltage drops to zero after a large voltage spike. A similar situation is seen when the system operates at 25 Hz and 41 Hz.

While the system is operating at 34 Hz, it can be seen in the FFT analysis that the values of the harmonics around the expected resonance frequency increase. When the system operates at 25 Hz and 41 Hz, the state is beyond a harmonic amplification, a conflict between the harmonics and the resonance frequency is observed. Also, when the operating frequency is 16 Hz, a similar conflict occurs, and insomuch that the THD observed over a time of 10 periods exceeds 100%. Therefore, it can be understood that the problems observed in the system at some frequencies, such as voltage drop to zero and the motor not producing torque, are the conflict of harmonics and resonance frequency.

According to the FFT results, it can be seen that the harmonics $(6n \pm 1)$ specified in formula (2.4) are created in the motor terminal voltage. Furthermore, as can be seen from the rise of the harmonics in the FFT analysis, the resonance frequency when the motor is idle during acceleration is around 2730 Hz as predicted in Subchapter 3.2.2. Hence, the conflict situation can be verified analytically according to formula (2.4) and resonance frequency as follows.

If $f = 16 \text{ Hz}$;

$$f_{169} = (6 \times 28 + 1) \times 16 = 2672 \text{ Hz}$$

$$\underline{f_{167} = (6 \times 28 - 1) \times 16 = 2704 \text{ Hz}}$$

$$f_{175} = (6 \times 29 + 1) \times 16 = 2768 \text{ Hz}$$

$$f_{173} = (6 \times 29 - 1) \times 16 = 2800 \text{ Hz}$$

When operating at 16 Hz, it is seen that the 167th harmonic of the system is close to the resonance frequency.

If $f = 25 \text{ Hz}$;

$$f_{109} = (6 \times 18 + 1) \times 25 = 2675 \text{ Hz}$$

$$f_{107} = (6 \times 18 - 1) \times 25 = 2725 \text{ Hz}$$

$$f_{115} = (6 \times 19 + 1) \times 25 = 2825 \text{ Hz}$$

$$f_{113} = (6 \times 19 - 1) \times 25 = 2875 \text{ Hz}$$

When the system operates at 25 Hz, the 107th harmonic corresponds to the surroundings of the resonance frequency.

If $f = 34 \text{ Hz}$;

$$f_{79} = (6 \times 13 + 1) \times 34 = 2618 \text{ Hz}$$

$$f_{77} = (6 \times 13 - 1) \times 34 = 2686 \text{ Hz}$$

$$f_{85} = (6 \times 14 + 1) \times 34 = 2822 \text{ Hz}$$

$$f_{83} = (6 \times 14 - 1) \times 34 = 2890 \text{ Hz}$$

The system operating at 34 Hz has no harmonic around the expected resonance frequency.

If $f = 41 \text{ Hz}$;

$$f_{67} = (6 \times 11 + 1) \times 41 = 2665 \text{ Hz}$$

$$f_{65} = (6 \times 11 - 1) \times 41 = 2747 \text{ Hz}$$

$$f_{73} = (6 \times 12 + 1) \times 41 = 2911 \text{ Hz}$$

$$f_{71} = (6 \times 12 - 1) \times 41 = 2993 \text{ Hz}$$

When the system operates at 41 Hz, it can be seen that the 65th harmonic value is close to the expected resonance frequency value.

It is understood that also analytically, the situation that causes problems during acceleration of the motor in the system is that the harmonics correspond to around the resonance frequency. The detection of all operating frequencies in which these problems may occur can be done with the program in Appendix 4. Accordingly, the regions (1 Hz, 2 Hz, 3 Hz, 4 Hz, 5 Hz, 6 Hz, 8 Hz, 25 Hz, 27 Hz, 30 Hz, 42 Hz) that fundamental harmonics can correspond between 2725 Hz and 2735 Hz is marked in red in Figure 3.19. Since similar problems can be experienced at frequencies close to the expected resonance frequency, also harmonics corresponding to the range of

2695 to 2750 Hz have been examined with this program and the regions (7 Hz, 9 Hz, 10 Hz, 11 Hz, 12 Hz, 13 Hz, 14 Hz, 15 Hz, 16 Hz, 17 Hz, 18 Hz, 19 Hz, 20 Hz, 23 Hz, 24 Hz, 28 Hz, 32 Hz, 33 Hz, 37 Hz, 38 Hz, 41 Hz, 45 Hz, 46 Hz) are marked in yellow in Figure 3.19. The regions where a resonance-induced problem is not expected are marked green. Accordingly, the regions that the system can face the problem are simply as follows.



Figure 3.19 Resonance status during start operation of the system

At lower frequencies, because there are more harmonics around the resonance frequency, the risk of conflict is greater. Resonance is manifested in the form of more torque and speed fluctuations since the system cannot yet come to equilibrium and generate high voltage while the system is operating at a low frequency. However, these waves will damage the system and, as in frequency 16, can cause overvoltages of extreme magnitude after some time. Also, at dangerous high frequencies, the system should not be held for a long time. The danger that resonance can create can be understood from the fact that the percentage value of the harmonics at resonance frequency exceeds the percentage value of the fundamental frequency of the system such as Figure 3.15.

By shifting or eliminating the resonance frequency of the system, the number of dangerous frequencies can be reduced. A filter can be placed on the AC grid side, which is the source of the problem. This is more convenient.

CHAPTER FOUR

SYSTEM PROTECTION AGAINST RESONANCE

The fluctuations in motor terminal voltage, torque, and speed, as well as the magnitude of the harmonic components and THD observed in the analysis. The system need should be protected against resonance. In order to protect the system, suitable parameters can be selected at the design stage, taking into account the resonance conditions. Furthermore, it may be an effective protection method not to hold the system for a long time at the frequencies determined in the analysis when the resonance may occur, by identifying an appropriate starting and working strategy. Other than that, methods may be selected to shift the resonance frequency detected in the analysis, to reduce its effect, or to eliminate it completely.

In order to reduce the effect of resonance and harmonics and to ensure that the system operates more reliable according to the needs, a filter on the AC grid in the motor side can be installed. Two types of filters, LCL and C-type, can be used to protect the analyzed system.

4.1 LCL Filter

In medium or large-scale power systems, the LCL filter can be used to increase power transfer and system efficiency. (Reznik, Simoes, Al-Durra & Muyeen, 2014) This filter, as shown in Figure 4.1, consists of wye connected groups that contain inductance, capacitance, and a damping resistor. It can also be created in different configurations with delta connections. (Reznik et al., 2014) They provide a better harmonic attenuation with components whose total size is smaller than simple L and LC filters (Rockhill, Liserre, Teodorescu, & Rodriguez, 2011). Therefore, they cause a lower voltage drop and they require less cost at the same time. Besides, they have a mitigating effect not only on low-frequency harmonics but also on the whole harmonic orders (Rockhill et al., 2011).

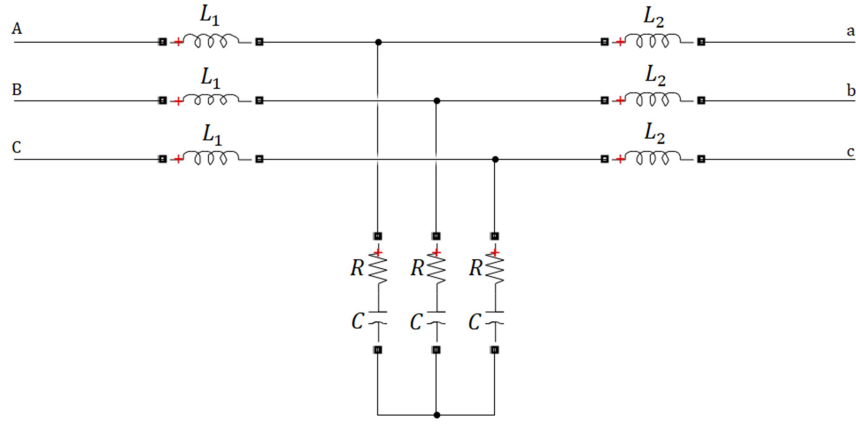


Figure 4.1 The structure of LCL filter

There is a step-up transformer in the analyzed system. Since the effects of the resonance frequency and the effects of the increasing harmonic components are seen on the motor terminal voltages as can be understood from the analyzes, it can be preferred to put the filter between step-up transformer and motor in this system as shown in Figure 4.2.

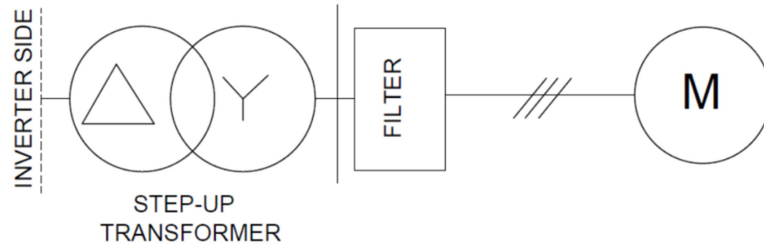


Figure 4.2 The filter position

The base impedance, inductance and capacitance values of the section where the filter is placed must be known in order to design the filter. As stated in Section 2.3, the base values of the first zone where the filter is placed are as follows.

$$Z_{B1} = 32.67 \, \Omega$$

$$L_{B1} = 0.1039 \, H$$

$$C_{B1} = 9.7432 \times 10^{-5} \, F$$

Some criteria must be met before the design is appropriate. In order to avoid excessive voltage drop, the total available inductance size can be limited as follows (Huang, Blaabjerg, Yang & Wu, 2013).

$$L_1 + L_2 \leq 0.1 \text{ pu} \quad (4.1)$$

According to the above formula;

$$\frac{L_1 + L_2}{0.1039} \leq 0.1 \text{ pu}$$

$$L_1 + L_2 \leq 0.01039 \text{ H}$$

The maximum ripple in current is generally considered to be lower than 40% in such inverter systems (Huang et al., 2013). Accordingly, by selecting an acceptable ripple value in this range, the inductance value on the inverter side is determined. The following formula can be used for this (Huang et al., 2013; Wang, Ye, Sinha & Yuan, 2003).

$$\Delta I_{max} = \frac{1}{8} \times \frac{V_{dc}}{L_1 f_{sw}} \quad (4.2)$$

According to equation (2.1);

$$V_{dc} = \frac{6\sqrt{2} \times 3300}{\pi \times \frac{3300}{400}} \cos 0 = 1080.38 \text{ V}$$

According to equation (4.2);

$$\frac{20}{100} \times \frac{10^6}{3 \times 3300} = \frac{1}{8} \times \frac{1080.38}{L_1 \times 2000}$$

$$L_1 = 3.3424 \times 10^{-3} \text{ H}$$

Where $\Delta I_{max} = 20\%$

The capacitance value to be used in the filter may change the power factor of the system. Usually the acceptable exchange rate is 5% (Huang et al., 2013). But the capacitance (C) limit can be changed if there is no additional compensation components in the system (Reznik et al., 2014; Wang et al., 2003). By using a lower inductance value, the capacity value can be increased further (Araujo, Engler, Sahan, & Antues, 2007). Accordingly, the capacitance limit is temporarily selected as 20%. Therefore, the capacitance value can be calculated by the following formula.

$$C \leq 0.2C_{B1} \quad (4.3)$$

According to the above formula;

$$C \leq (0.2 \times 9.7432 \times 10^{-5})$$

$$C \leq 1.9486 \times 10^{-5} F$$

Picture 5 shows that the harmonic current is also produced at the inverter output. The L_2 value can be selected to limit this. The following formula can be used (Reznik et al., 2014).

$$L_2 = \frac{\sqrt{\frac{1}{k_a^2} + 1}}{C \omega_{sw}^2} \quad (4.4)$$

According to above formula;

$$L_2 = \frac{\sqrt{\frac{1}{0.25^2} + 1}}{1.9486 \times 10^{-5} (2 \times \pi \times 2000)^2}$$

$$L_2 = 1.6255 \times 10^{-3} H$$

where $k_a = 0.25$ (desired attenuation factor)

A damping resistor can be added to the system to reduce fluctuations during switching and to prevent filter-induced resonance. Before that, it should be ensured that the resonance frequency that may be caused by the filter parameters is far from the switching frequency. This problem can be avoided by observing the range specified in equation (4.6) (Reznik et al., 2014). Araujo et al. (2007) have stated that the damping resistance value could be one third of the value of the capacitive reactance at the resonance frequency according to the power loss limit they determined and if the resistance value increases, this limit can be reduced. They also stated that the damping will be ineffective when the resistance value is reduced. On the other hand, it has been argued that the greater resistance value provides more effective damping but it can bring along the problem such as the greater power loss and the worse harmonic attenuation (Wang et al., 2003). The value of the damping resistance can be calculated by taking into account the capacitive reactance value at

the moment of resonance as indicated in formula (4.7) (Araujo et al., 2007) and considering that the situation can be adjusted according to the result obtained.

$$\omega_r = \sqrt{\frac{L_1 + L_2}{L_1 L_2 C}} \quad (4.5)$$

$$10f \leq f_r \leq 0.5f_{sw} \quad (4.6)$$

$$R = \frac{1}{3\omega_r C} \quad (4.7)$$

According to formula (4.5);

$$\omega_r = \sqrt{\frac{3.3424 \times 10^{-3} + 1.6255 \times 10^{-3}}{3.3424 \times 10^{-3} \times 1.6255 \times 10^{-3} \times 1.9486 \times 10^{-5}}}$$

$$\omega_r = 6850.186 \text{ rad/s}$$

Hence,

$$f_r = 1090 \text{ Hz}$$

According to the formula (4.6), it can be said that approximately f_r is acceptable. Therefore, according to formula (4.7), the resistor value to be placed in series to capacity is as follows.

$$R = \frac{1}{3 \times 6850.186 \times 1.9486 \times 10^{-5}}$$

$$R = 2.4972 \Omega$$

According to the selected filter parameters specified in Table 4.1, the obtained motor terminal voltage and FFT analysis are as in Figure 4.3.

Table 4.1 Parameters of the LCL filter

Parameters of the Filter	First State	Final State
$L_1 (mH)$	3.3424	1.6712
$L_2 (mH)$	1.6255	0.8125
$C (\mu F)$	19.486	38.972
$R (\Omega)$	2.4972	2.4972

It has been observed that the harmonic rise around the predicted resonance frequency decreases thanks to the selected parameters. But that's not exactly enough, in most cases. The system may need a voltage waveform more similar to the sine, and lower total harmonic distortion. Thus, by renewing the parameters, a more effective resonance attenuation can be achieved and the system can be improved.

For proper operation of the filter, the parameters can be renewed by complying with the resonance frequency limits specified in equation (4.6) and the total impedance limit specified in equation (4.1). For this purpose, the current limit level is kept around 40% and the L_1 impedance level is halved and thus the capacity (C) value is doubled. In addition, according to the determined new capacity value and equation (4.4), the value of inductance L_2 is also halved. In this case, the value of the dumping resistance is kept constant in order not to reduce its effect and not to increase the power loss. The new status of the parameters is as follows.

$$L_1 = \frac{\frac{1}{8} \times \frac{1080.38}{2000}}{\frac{40}{100} \times \frac{10^6}{3 \times 3300}}$$

$$L_1 = 1.6712 \times 10^{-3} H$$

Where $\Delta I_{max} = 40\%$

Capacitance is,

$$C = 1.9486 \times 10^{-5} \times 2 = 3.8972 \times 10^{-5} F$$

Hence,

$$L_2 = \frac{\sqrt{\frac{1}{0.25^2} + 1}}{3.8972 \times 10^{-5} \times (2 \times \pi \times 2000)^2} = 8.1245 \times 10^{-4} H$$

According to the calculated new L_1 , L_2 and C values;

$$\omega_r = \sqrt{\frac{1.6712 \times 10^{-3} + 8.1245 \times 10^{-4}}{1.6712 \times 10^{-3} \times 8.1245 \times 10^{-4} \times 3.8972 \times 10^{-5}}} = 6851 \text{ rad/s}$$

Hence,

$$f_r = 1090 \text{ Hz}$$

Again, it can be seen from the above that it is approximately within the specified resonance limits. Furthermore, as can be seen in the calculation below, the new total inductance value did not exceed the limit specified in equation (4.1).

$$1.6712 \times 10^{-3} + 8.1245 \times 10^{-4} = 2.4836 \times 10^{-3} H$$

$$L_1 + L_2 \leq 0.01039 H$$

According to the new parameters in Table 4.1, voltage waveform and FFT results are obtained as in Figure 4.4. It can be seen from the results that the voltage waveform has been improved, harmonics has been attenuated more and total harmonic distribution has been decreased further.

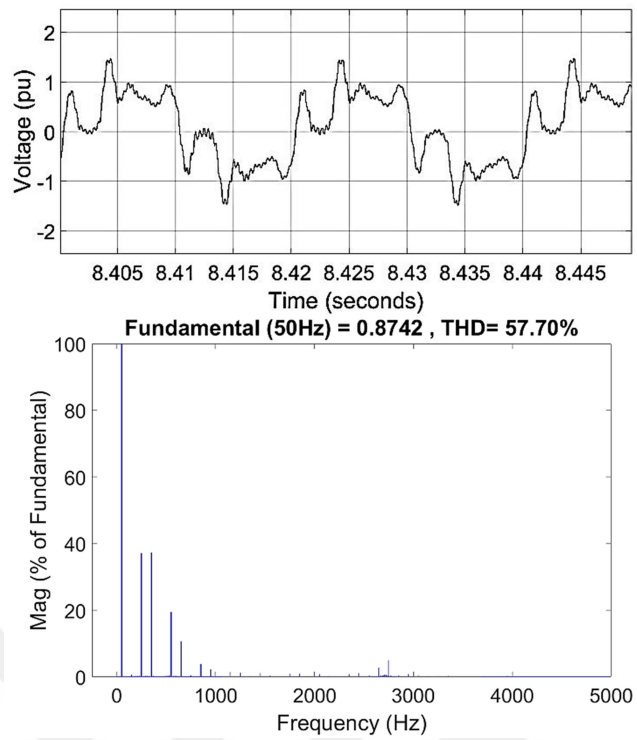


Figure 4.3 Motor terminal voltage and FFT analysis

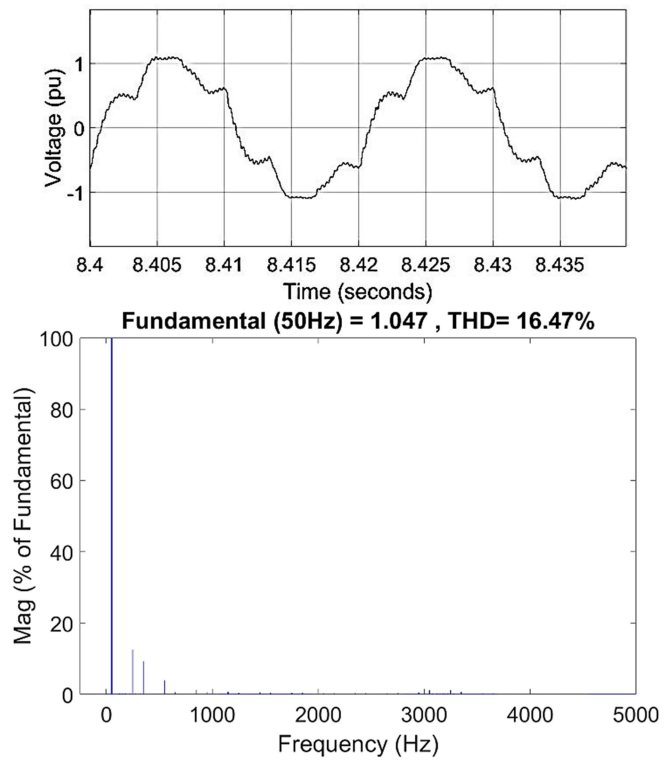


Figure 4.4 Motor terminal voltage and FFT analysis in last state

4.2 C-Type Filter

C-type filter was first used in HVDC systems. Later, it was adapted to many power systems such as green power and continued to be used (Xiao, Zhao & Mao, 2004). That filter is suitable for working with power electronic devices and are very effective in eliminating the characteristic harmonics arising from the structure of these. It also has a wide operating range and can filter not only low order harmonics but also high-frequency harmonics (Klempka, 2012). The structure of the 3-phase C-type filter is as in Figure 4.5.

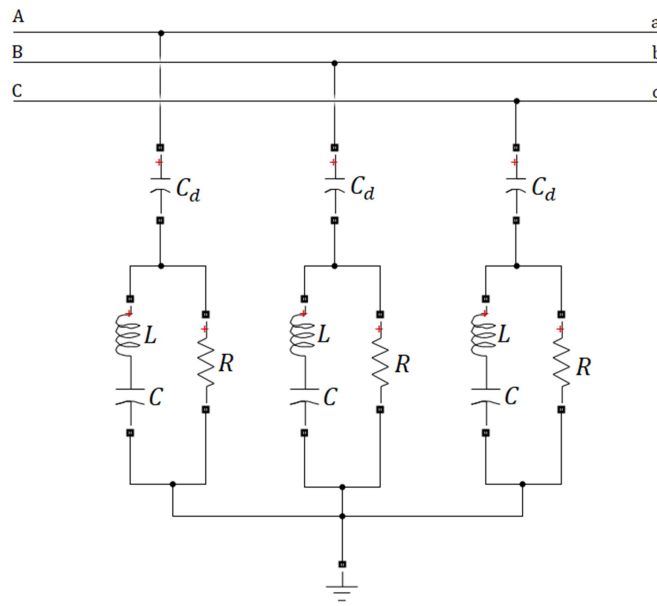


Figure 4.5 C-Type filter structure

The design of this filter is generally based on two conditions: reactive power output and fundamental frequency. However, methods including tuning frequency have been proposed (Zhang, Wang, Xu & Sittther, 2018). Accordingly, in order to design the filter, firstly the tuning frequency, reactive power, and quality factor can be determined (Xiao et al., 2004).

According to the analysis, the expected resonance frequency value in normal operation is approximately 2850 Hz. With this in mind, in order to protect the system from the harmful effects of overvoltage, the tuning frequency can be determined as follows.

In the FFT analysis shown in Figure 9, it is seen that the overvoltages formed around the 57st harmonic. In order to protect the system from the harmful effects of overvoltage, the method of eliminating the harmonic in which the resonance occurs can be used.

$$f_0 = 2850 \text{ Hz}$$

The harmonic order corresponding to the tuning frequency can be calculated with equation (4.8).

$$h_0 = \frac{f_0}{f} \quad (4.8)$$

According to above formula;

$$h_0 = \frac{2850}{50} = 57$$

25% of the base power value was found sufficient to meet the reactive power requirement of the system. The system rated voltage, and the assumed quality factor is as follows.

$$Q_N = 0.25 \times 10^6 \text{ MVAR}$$

$$U_N = 3.3 \text{ kV}$$

$$Q = 10$$

The value of the components of the filter can be calculated according to these selected parameters. To alleviate the harmonics of the fundamental frequency in general, capacitive reactance and capacitance(C_d) values can be calculated as specified in equation (4.9) and equation (4.10) respectively, depending on the specified reactive power and the nominal voltage of the system (Chen, Chen & Cotmick, 2004).

$$X_{C_d} = \frac{3U_N^2}{Q_N} \quad (4.9)$$

$$C_d = \frac{1}{2\pi f X_{C_d}} \quad (4.10)$$

According to equation (4.9) and equation (4.10);

$$X_{C_d} = \frac{3 \times 3300^2}{0.25 \times 10^6} = 130.68 \Omega$$

$$C_d = \frac{1}{2 \times \pi \times 50 \times 130.68} = 2.4358 \times 10^{-5} F$$

Other parameters of the filter are calculated from the h_0 value given by the tuning frequency. The components, whose value is determined according to the tuning frequency, ensure that the filter not only attenuates the basic harmonics but also protects the system within a certain frequency range where problems such as resonance may be encountered. Thus, the damping resistance value can be calculated according to formula (4.11) (Chen et al., 2004). It is the factor that determines the response of the system, especially at high frequencies (Zhang et al., 2018).

$$R = \frac{1}{2\pi f C_d h_0} \quad (4.11)$$

According to above formula;

$$R = \frac{1}{2 \times \pi \times 50 \times 2.4358 \times 10^{-5} \times 57} = 2.2926 \Omega$$

The inductance value of LC branch connected parallel to damping resistance can be calculated by using equation (4.12).

$$L = mR^2 C_d \quad (4.12)$$

Where

$$m = \frac{1}{Q}$$

According to above formula;

$$L = 0.1 \times 2.2926^2 \times 2.4358 \times 10^{-5} = 1.2803 \times 10^{-5} H$$

To avoid any resonance, also the capacitance value of the LC branch can be calculated by taking source from the angular frequency specified in equation (4.13).

$$\omega = \frac{1}{\sqrt{LC}} \quad (4.13)$$

According to formula (4.13);

$$C = \frac{1}{\omega^2 L} = \frac{1}{(2 \times \pi \times 50)^2 \times 1.2803 \times 10^{-5}} = 0.7904 F$$

Table 4.2 Parameters of the C-type filter

Parameters of the Filter	
$C_d (F)$	2.4358×10^{-5}
$L (H)$	1.2803×10^{-5}
$C (F)$	0.7904
$R (\Omega)$	2.2926

With these calculated parameters are given Table 4.2, the motor terminal voltages and the FFT are obtained in Figure 4.6. It can be seen that the harmonics around the 57th harmonic can be eliminated and generally an attenuation on the harmonics is achieved compared with the results of the unfiltered system given in Figure 3.6. Besides that, there is an improvement in voltage waveform and a reduction in total harmonic distortion.

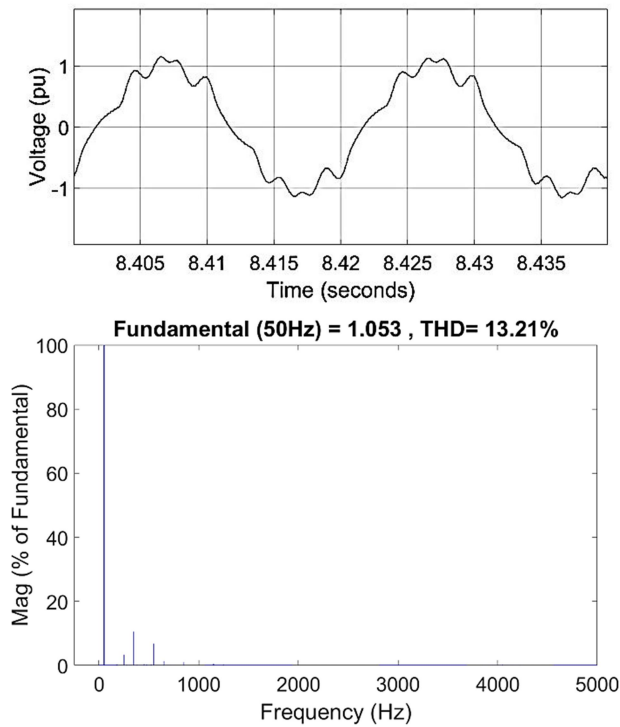


Figure 4.6 Motor terminal voltage and FFT analysis

CHAPTER FIVE

CONCLUSIONS

In the system, there are elements that may have high disturbance effects such as power electronic circuits containing nonlinear switching elements, long cables with high capacitive effect, transformers containing magnetizing circuits and motor related to external elements such as load. As predicted, it is observed that this complex structure of the system constitutes the resonance conditions and exceeds the characteristic harmonics arising from the structure of the six-step driver. Resonance causes overvoltages at motor terminals and fluctuations in torque and speed. If the resonance frequency coincides with the characteristic harmonics, the effects of these overvoltages are more destructive and the system cannot recover.

The impedance of the system is the most important parameter in determining the resonance conditions. From this, the resonance frequency can be determined analytically and with simulations. Accordingly, it was observed that the cable length and slip change the resonance conditions. Increasing the length of the cable may cause greater problems of resonance. On the other hand, the information provided by the slip about resonance is important especially in order to predict the problems that may be encountered in idle work.

The elements of this system, in particular, the cables and the motor, can withstand against over-voltages and overheating, up to a certain limit and a certain period of time, depending on the properties of the materials from which they are produced. Resonance may damage the insulation of these elements. It also may cause the drive to operate undesired. The unusual conditions caused by resonance detected in the analysis may even result in motor burnout. Therefore, it is necessary to protect the system. LCL and C-type filters can be used for this purpose. It has been observed that the problems identified in the analyzes can be reduced with these filters.

REFERENCES

- Akpinar, E., & Pillay, P. (1993). Motor drive performance during supply disturbances. In *Large process industry motor drive performance and power quality analysis* (1-66). Palo Alto: Electric Power Research Institute.
- Akpinar, E., & Pillay, P. (1994). Modeling and performance of a 120 degree square-wave inverter/induction machine drive. *Journal of Electrical Power System Research*, 31(1), 21-29.
- Araujo, S. V., Engler, A., Sahan, B., & Antunes, F. L. M. (2007). LCL filter design for grid-connected NPC inverters in offshore wind turbines. *7th International Conference on Power Electronics*, 1133-1138.
- Baby, B. K., & George, S. (2012). Torque ripple reduction in BLDC motor with 120 degree conduction inverter. *Annual IEEE India Conference (INDICON)*, 1116-1121.
- Bertoldi, F., Pathmanathan, M., Kanchan, R. S., Spiliotis, K., & Driesen, J. (2018). Quasi-two-level converter for overvoltage mitigation in medium voltage drives. *International Power Electronics Conference (IPEC)*, 488-494.
- Boglietti, A., Ferraris, P., Lazzari, M., & Profumo, F. (1993). Effects of different modulation index on the iron losses in soft magnetic materials supplied by PWM inverter. *IEEE Transactions on Magnetics*, 29(6), 3234-3236.
- Cataliotti, A., Daidone, A., Sanacore, G. & Tinè, G. (2008). Characterization of medium voltage cables for power line communication. *IEEE Transactions on Power Delivery*, 23(4), 1896-1902.
- Chen, Q., Chen, Z., & McCormick, M. (2004). The application and optimization of C-type filter in a combined harmonic power filter. *IEEE 35th Annual Power Electronics Specialists Conference*, 2, 1041-1045.
- Diyoke, G. C., Okeke, C., & Aniagwu, U. (2016). Different methods of speed control of three-phase asynchronous motor. *American Journal of Electrical and Electronic Engineering*, 4(2), 62-68.

- Endrejat, F., Burmeister, P., & Pillay, P. (2009). Large adjustable speed and soft-started drives with long cable lengths. *Conference Record PCIC Europe*, 153-162.
- Endrejat, F., & Pillay, P. (2009). Resonance overvoltages in medium-voltage multilevel drive systems. *IEEE Transactions on Industry Applications*, 45(4), 1199-1209.
- Holtz, J., Lotzkat, W., & Khambadkone, A. M. (1993). On continuous control of PWM inverters in the overmodulation range including the six-step mode. *IEEE Transactions on Power Electronics*, 8(4), 546-553.
- Huang, M., Blaabjerg, F., Yang, Y., & Wu, W. (2013). Step by step design of a high order power filter for three-phase three-wire grid-connected inverter in renewable energy system. *4th IEEE International Symposium on Power Electronics for Distributed Generation Systems (PEDG)*, 1-8.
- Hussain, H. A., Anvari, B., & Toliyat, H. A. (2017). A control method for linear permanent magnet electric submersible pumps in a modified integrated drive-motor system. *IEEE International Electric Machines and Drives Conference (IEMDC)*, 1-7.
- Hussen, M. (2009). Difference between of PWM strategies for inverter fed induction motor. *Journal of Engineering*, 15(3), 4009-4025.
- Kerkman, R. J., Rowan, T. M., Leggate, D., & Seibel, B. J. (1995). Control of PWM voltage inverters in the pulse dropping region. *IEEE Transactions on Power Electronics*, 10(5), 559-565.
- Klempka, R. (2012). A new method for the C-type passive filter design. *Przegląd Elektrotechniczny (Electrical Review)*, 7a, 277-281.
- Krause, P.C., Wasynczuk, O., & Sudhoff, S.D. (1995). *Analysis of electric machinery*. New York: The Institute of Electrical and Electronics Engineers, Inc.
- Liang, X., & Fleming, E. (2013). Electrical submersible pump systems: evaluating their power consumption. *IEEE Industry Applications Magazine*, 19(6), 46-55.

- Liang, X., Kar, N. C., & Liu, J. (2014). Load filter design method for medium-voltage drive applications in electrical submersible pump systems. *IEEE Transactions on Industry Applications*, 51(3), 2017-2029.
- Mohan, N., Undeland, T.M., & Robbins, W.P. (2003). *Power electronics: converters, applications, and design* (3rd ed.). USA: John Wiley & Sons, Inc.
- Morley, L.A. (1990). *Mine power systems*. Washington. DC: U.S. Government Printing Office.
- Narayanan, G., & Ranganathan, V.T. (1998). Synchronised bus-clamping PWM strategies based on space vector approach for modulation up to six-step mode. *International Conference on Power Electronic Drives and Energy Systems for Industrial Growth*, 2, 996-1001.
- Narayanan, G., & Ranganathan, V. T. (2002). Extension of operation of space vector PWM strategies with low switching frequencies using different overmodulation algorithms. *IEEE Transactions on Power Electronics*, 17(5), 788-798.
- Qian, K., Sun, Y.N., Zheng, S., Du, W.S., Li, J.N., Pei, G.Z., & et al. (2018). Research and application of key technology of electric submersible plunger pump. *IOP Conference Series: Materials Science and Engineering*, 372(1), 12-24.
- Rashid, M.H. (2013) *Power electronics: devices, circuits, and applications* (4th Ed.). London: Pearson.
- Reznik, A., Simões, M.G., Al-Durra, A., & Mueen, S.M. (2014). LCL filter design and performance analysis for grid-interconnected systems. *IEEE Transactions on Industry Applications*, 50(2), 1225-1232.
- Rockhill, A. A., Liserre, M., Teodorescu, R., & Rodriguez, P. (2011). Grid-filter design for a multimewatt medium-voltage voltage-source inverter. *IEEE Transactions on Industrial Electronics*, 58(4), 1205-1217.
- Rodríguez, J., Pontt, J., Silva, C., Musalem, R., Newman, P., Vargas, R., & Fuentes, S. (2006). Resonances and overvoltages in a medium-voltage fan motor drive with

- long cables in an underground mine. *IEEE Transactions on Industry Applications*, 42(3), 856-863.
- Saadat, H. (2010). *Power system analysis* (3rd ed.). USA: PSA Publishing.
- Spijker, H.V., & Ungemach, P. (2016). *Definition of electrosubmersible pump (ESP) design and selection workflow*. Kennisagenda: Kas als Energiebron.
- Sudhoff, S. D., & Krause, P. C. (1990). Operating modes of the brushless DC motor with a 120 degrees inverter. *IEEE Transactions on Energy Conversion*, 5(3), 558-564.
- Sueker, K.H. (2005). *Power electronics design: a practitioner's guide*. Burlington: Elsevier.
- Sundaram, M., Anand, M., Vinod, B., & Mounya, N. (2016). Design and development of 5-HP BLDC motor for submersible application. *Asian Journal of Research in Social Sciences and Humanities*, 6(12), 483-496.
- Takacs, G. (2009). *Electrical submersible pumps manual: design, operations, and maintenance*. Oxford: Gulf Professional Publishing.
- Thue, W.A. (2003). *Electrical power cable engineering*. New York: Marcel Dekker, Inc.
- Thorsen, O.V. & Dalva, M. (2001). Combined electrical and mechanical model of electric submersible pumps. *IEEE Transactions on Industry Applications*, 37(2), 541-547.
- Wang, M. (2010). *Understandable electric circuits*. Stevenage: The Institution of Engineering and Technology.
- Wang, T. C., Ye, Z., Sinha, G., & Yuan, X. (2003). Output filter design for a grid-interconnected three-phase inverter. *IEEE 34th Annual Conference on Power Electronics Specialist*, 2, 779-784.
- Williams, B.W. (2006). *Principles and elements of power electronics: devices, drivers, applications and passive components*. Glasgow: Barry W. Williams.

- Xiao, Y., Zhao, J., & Mao, S. (2004). Theory for the design of C-type filter. *IEEE 11th International Conference on Harmonics and Quality of Power*, 11-15.
- Xu, L. & Ye, L. (1995). Analysis of a novel stator winding structure minimizing harmonic current and torque ripple for dual six-step converter-fed high power AC machines. *IEEE Transactions on Industry Applications*, 31(1), 84-90.
- Zhang, G., Wang, Y., Xu, W., & Sitther, E. (2018). Characteristic parameter based detuned C-type filter design. *IEEE Power and Energy Technology Systems Journal*, 5(2), 65-72.
- Zheng, G. & Wang, S.W. (2013). Application of rodless pump in gproduction of downhole linear motor and matching techniques in ultra-low permeability reservoirs of Changqing oil field. *Journal of Oil and Gas Technology*, 35, 158-178.

APPENDICES

Appendix 1: MATLAB Script for Per-unit Data

```
% All values are given on the same system base MVA

%% Line data
% 1: Line no
% 2: Resistance (pu)
% 3: Inductance (pu)
% 4: Capacitance (pu)
% 5: Base Voltage (KV)
% 6: Base Power(MVA)

%      1      2      3      4      5      6
line=[
    1    0.0118  3.378e-3  3.264e-3  3.3    1/3
    2    0.1571  0.1859   8.852e-5  0.4    1/3
    3    0.1571  0.1859   8.852e-5  0.4    1/3
    4    0.0238  0.0697   2.764e-4  0.63   1/3
    5    0.0118  3.378e-3  3.264e-3  3.3    1/3  ];

zbase=line(:,5).^2./line(:,6);
line(:,2)=line(:,2).*zbase;
line(:,3)=line(:,3).*zbase/(2*pi*f);
line(:,4)=line(:,4)./(zbase*2*pi*f);

%% Source data
% 1: Resistance (pu)
% 2: Inductance (pu)
% 3: Base Voltage (KV)
% 4: Base Power(MVA)

%      1      2      3      4
source=[0.082  0.4783  3.3/sqrt(3)    1/3];

zbase2=source(:,3).^2./source(:,4);
source(:,1)=source(:,1).*zbase2;
source(:,2)=source(:,2).*zbase2/(2*pi*f);

%% Smoothing capacitance data
% 1: Capacitance (pu)
% 2: Base Voltage (KV)
% 3: Base Power(MVA)
```

```

%           1           2           3

smooth=[18.7035      0.63      1/3];

zbase3=smooth(:,2).^2./smooth(:,3);
smooth(:,1)=smooth(:,1)./(zbase3*2*pi*f);

%% Transformer data
%% Simulink pu transformer block can be used in the simulation
instead.
% 1: R1 (pu)
% 2: L1 (pu)
% 3: RM (pu)
% 4: LM (pu)
% 5: R2 (pu)
% 6: L2 (pu)
% 7: Winding 1 Base Voltage (KV)
% 8: Winding 2 Base Voltage (KV)
% 9: Base Power (MVA)

%           1           2           3           4           5           6           7           8
9
tr=[10^(-5)      0.02      10^(-5) 0.02      100      100      0.63
3.3/sqrt(3) 1/3];

zbasew1=tr(:,7).^2./tr(:,9);
zbasew2=tr(:,8).^2./tr(:,9);

tr(:,1)=tr(:,1)*zbasew1;
tr(:,2)=tr(:,2).*(zbasew1/(2*pi*f));
tr(:,5)=tr(:,5).*(zbasew1/(2*pi*f));
tr(:,6)=tr(:,6).*(zbasew1/(2*pi*f));
tr(:,3)=tr(:,3).*(zbasew2/(2*pi*f));
tr(:,4)=tr(:,4).*(zbasew2/(2*pi*f));

%% 3-winding Transformer data
%% Simulink pu transformer block can be used in the simulation
instead.
% 1: R1 (pu)
% 2: L1 (pu)
% 3: RM (pu)
% 4: LM (pu)
% 5: R2 (pu)
% 6: L2 (pu)
% 7: R3 (pu)
% 8: L3 (pu)
% 9: Winding 1 Base Voltage (KV)
% 10: Winding 2 Base Voltage (KV)
% 11: Winding 3 Base Voltage (KV)
% 12: Base Power (MVA)

```

```

%      1      2      3      4      5      6      7      8      9
% 10      11     12

tr2=[0.0006 0.04 0.0006 0.04 0.0006 0.04 500 500 3.3/sqrt(3)
0.4/sqrt(3) 0.4 1/3];

zbasep1=tr2(:,9).^2./tr2(:,12);
zbases1=tr2(:,10).^2./tr2(:,12);
zbases2=tr2(:,11).^2./tr2(:,12);

tr2(:,1)=tr2(:,1).*zbasep1;
tr2(:,2)=tr2(:,2).*zbasep1/(2*pi*f);
tr2(:,7)=tr2(:,7).*zbasep1;
tr2(:,8)=tr2(:,8).*zbasep1/(2*pi*f);
tr2(:,3)=tr2(:,3).*zbases1;
tr2(:,4)=tr2(:,4).*zbases1/(2*pi*f);
tr2(:,5)=tr2(:,5).*zbases2;
tr2(:,6)=tr2(:,6).*zbases2/(2*pi*f);

%% Induction motor data
%% Simulink pu motor block can be used in the simulation
instead.
% 1: Rs (pu)
% 2: Ls (pu)
% 3: Rr (pu)
% 4: Lr (pu)
% 5: Lm (pu)
% 6: Base Voltage (KV)
% 7: Base Power (MVA)

%      1      2      3      4      5      6      7
m=[0.0894 0.2238 0.1137 0.2746 5.0476 3.3/sqrt(3) 1/3];

zbasem=m(:,6).^2./m(:,7);

m(:,1)=m(:,1).*zbasem;
m(:,2)=m(:,2).*zbasem/(2*pi*f);
m(:,3)=m(:,3).*zbasem;
m(:,4)=m(:,4).*zbasem/(2*pi*f);
m(:,5)=m(:,5).*zbasem/(2*pi*f);

```

Appendix 2: MATLAB Script for Calculation of the Resonance Frequency

```
l=5;

%motor
Rs=m(1,1);
Lls=m(1,2);
Rr=m(1,3);
Llr=m(1,4);
Lm=m(1,5);
s=0.042;

%transformer
R1=tr(1,1);
L1=tr(1,2);
R2=tr(1,3);
L2=tr(1,4);

%cable
R5=line(5,2)*l;
L5=line(5,3)*l;
C=line(5,4)*l;

a=0.63/(3.3/sqrt(3));
Rt=R1+(a^2)*R2+R5;
Lt=L1+(a^2)*L2+L5;
Rtm=Rs+(Rr)/s;
Ltm=Lls+Llr;

%equation roots
c=-Lt*Lm*(Rtm)^2/C+(Rt)^2*Lm*(Rtm)^2-(Rt)^2*Ltm-
(Lt)^2*(Rtm)^2-Ltm*Lm*(Rt)^2;
b=-Lt*Lm*(Ltm)^2/C+(Rt)^2*Lm*(Ltm)^2+(Lt)^2*Lm*(Rtm)^2-
(Lt)^2*Lm*(Rtm)^2-(Lt)^2*(Ltm)^2-Ltm*Lm*(Lt)^2;
a=(Lt)^2*Lm*(Ltm)^2;
d=-(Rt)^2-(Rtm)^2;

polinom=[a 0 b 0 c 0 d];
wo=roots(polinom)
```

Appendix 3: MATLAB Script for Calculation of Total Parameters

```
l=5;

%motor
Rs=m(1,1);
Lls=m(1,2);
Rr=m(1,3);
Llr=m(1,4);
Lm=m(1,5);
s=0.042;

%transformer
R1=tr(1,1);
L1=tr(1,2);
R2=tr(1,3);
L2=tr(1,4);

%cable
R5=line(5,2)*1;
L5=line(5,3)*1;

a=0.63/(3.3/sqrt(3));
Rt=R1+(a^2)*R2+R5;
Lt=L1+(a^2)*L2+L5;
Rtm=Rs+(Rr)/s;
Ltm=Lls+Llr;

Lttotal=1/(1/Lt+1/Lm+1/Ltm)
R=1/(1/Rt+1/Rtm)
```

Appendix 4: MATLAB Script for Determination of Resonance Statuses

```
for i = 1:1000

    f=0;
    f1=2724; % f1=2695;
    f2=2736; % f2=2750;

    while f<=49
        f=f+1;

        n1=(6*i+1)*f;
        if (f1<n1) && (n1<f2);
            disp(f);
        end
        n2=(6*i-1)*f;

        if (f1<n2) && (n2<f2);
            disp(f);
        end
    end
end
```